

Analysis of Misorientation Relationships Between Austenite Parents and Twins



A.F. BRUST, S.R. NIEZGODA, V.A. YARDLEY, and E.J. PAYTON

The forward transformation from face-centered cubic austenite to body-centered cubic/tetragonal martensite in ferrous alloys can significantly influence the microstructure and mechanical properties of the material. Inferring possible high-temperature crystal orientations from observations of ambient temperature transformation microstructures is hindered by parent austenite–twin interactions and scatter in the orientation relationship. This creates a major limitation for studying variant selection phenomena and characterizing microstructural response to high-temperature thermomechanical processing conditions. In this work, composition tables are developed that detail the product variant boundary misorientation relationships for intra-parent, parent–twin, and twin–twin boundary intersections for the Kurdjumov–Sachs (KS), Nishiyama–Wassermann (NW), and an experimentally determined irrational orientation relationship. The frequently referenced KS and NW orientation relationships produce significantly different results from experimental observations. Furthermore, the introduction of a twin into the parent austenite introduces a substantially larger number of misorientation relationships when the orientation relationship is irrational. The effects of crystal symmetry on misorientation results are determined by considering both body-centered cubic and body-centered tetragonal martensite structures. Lastly, it is observed that some shared variants are found between twins and parents when assuming cubic symmetry but not tetragonal symmetry. The results and relationships may be useful towards accurate and consistent reconstructions of the parent austenite microstructure from observations of martensite.

<https://doi.org/10.1007/s11661-018-4977-5>

© The Minerals, Metals & Materials Society and ASM International 2018

I. INTRODUCTION

ON rapid cooling from the austenite phase field, austenite grains in steels with a carbon content of 0.6 pct or below decompose into martensite with 24 crystallographic variants of a lath morphology.^[1,2] At higher concentrations of carbon, a mixture of lath-like and plate-like martensite morphologies are observed.^[3–5] The martensitic transformation is athermal and often-times goes to full completion, where little to no parent austenite remains, before the material reaches room temperature. Microstructure characterization must therefore be performed solely on the transformed product, and the microstructure that existed in the

austenite phase field must be inferred from observations of the martensitic microstructure. Parent austenite grain structure plays a key role in the performance and properties of the transformed microstructure, such as the ductile to brittle fracture occurrence based on increasing prior austenite grain (PAG) diameter^[6,7] and the classification of creep and cavitation sites.^[8,9]

A transformed austenite grain consists of blocks of laths of two paired crystal variant orientations grouped into packets with a shared habit plane. Both packet and block boundaries are important hindrances to plastic deformation and crack propagation in steels.^[10–12] Therefore, the size and morphology of the prior austenite grains play a significant role in the mechanical properties of the transformed martensite. Furthermore, the prior austenite structure also contributes to the performance of the material through mechanisms such as impurity segregation at prior austenite grain boundaries, leading to temper embrittlement.^[13,14] Thus, the reconstruction of the austenite microstructure from the observable martensite is not only highly desired but also necessary for optimizing material processing and performance.

A.F. BRUST is with the Department of Materials Science and Engineering, The Ohio State University, Columbus, OH 43210. S.R. NIEZGODA is with the Department of Materials Science and Engineering, The Ohio State University, Department of Mechanical and Aerospace Engineering, The Ohio State University, Columbus, OH 43210. Contact e-mail: niezgoda.6@osu.edu V.A. YARDLEY is with the Eutectikon Computational Materials Consulting LLC, 33 Eastgate St., Stafford, ST16 2LZ, UK. E.J. PAYTON is with the Air Force Research Laboratory, Materials and Manufacturing Directorate, Dayton, OH 45433.

Manuscript submitted April 06, 2018.

Article published online November 21, 2018

In iron alloys, it is often assumed that the exhibited orientation relationship is close to one of the two “named” orientation relationships. When approximately 12 variants are observed, the Nishiyama–Wasserman (NW) orientation relationship is referenced^[15,16]:

$$\{111\}_\gamma // (011)_\alpha; \quad <\bar{1}\bar{1}2>_\gamma // <0\bar{1}1>_\alpha. \quad [1]$$

When 24 variants are observed, the Kurdjumov–Sachs (KS) orientation relationship is often cited^[17]:

$$\{111\}_\gamma // (011)_\alpha; \quad <\bar{1}01>_\gamma // <\bar{1}\bar{1}1>_\alpha. \quad [2]$$

In the actual orientation relationships, however, the parallel directions and planes are irrational. Cahn and Kalonji^[18] argued that, in regards to certain rotations, a symmetry-dictated energy extremum exists, although the symmetry does not specify whether the extremum is a minimum, maximum, or saddle point. They then determined that no symmetry-dictated energy extremum exists for KS, and that the NW orientation relationship produces either a maximum or a shallow minimum. Therefore, both of these cases (KS and NW) can be considered idealized orientation relationships. Deviations from exact parallelism have been characterized by Greninger and Troiano^[19] and are predicted by the phenomenological theory of martensitic transformations.^[20–27] Experimentally measured orientation relationships will always contain 24 variants but depart from KS or NW orientation relationships. The departure varies with composition and cooling rate.^[28,29] Anywhere from one to 24 variants can be observed in a prior austenite grain following transformation. Furthermore, it is well known that the martensite crystal structure is body-centered tetragonal (bct) or body-centered cubic (bcc). Which crystal structure is present depends on the concentration of carbon, typically taking the bcc form at less than 0.6 pct C, with an expanding c/a ratio with an increasing amount of C.^[30]

An improved understanding of the variant-to-variant misorientation relationships may be used to improve electron backscatter diffraction (EBSD)-based reconstruction techniques of the prior austenite phase. The prior austenite microstructure can significantly affect physical properties of the phase-transformed material through microstructure scale^[31] and potentially through crystallographic texture. In the present work, composition tables of the misorientation relationships between variants within a single prior austenite grain and its annealing twins are calculated for three separate orientation relationships: KS, NW, and one which has been experimentally determined,^[32] building off of the work by Cayron.^[33] It is currently not possible to accurately measure the c-axis extension that would distinguish bct from bcc at higher C content using EBSD (resulting in pseudosymmetry in the experimental results). As such, bct martensite in EBSD is typically indexed as bcc. To determine whether this has any impact on the misorientation data, both cubic (point group $m\bar{3}m$) and tetragonal (point group $4 / mmm$) symmetry are used to compute the misorientations in standalone composition tables.

II. MATERIALS AND METHODOLOGY

Starting from a single prior austenite orientation aligned with the sample reference frame (Bunge Euler angles of $\phi_1 = \Phi = \phi_2 = 0$), the four $\Sigma 3$ face-centered cubic annealing twin orientations were calculated from the four unique rotations of 60 deg about $<1\bar{1}1>$.

A number of experimentally observed orientation relationships have been determined from EBSD analysis of SEM and TEM characterized microstructures.^[1,28] For this paper, the experimentally measured orientation relationship was established based on the procedure outlined in references^[6,8,32,34] on a sample of low carbon steel, which may be expected to have a KS-like orientation relationship. The orientation relationship was determined through the use of measured ξ angles, with untwinned PAGs being identified and selected manually within a given micrograph range. The datasets were then rotated to coincide the PAG orientation with the sample reference frame, with the angular deviation between the primary axis of the rotation matrix and the axes of the closest Bain correspondence matrix representing the orientation relationship in terms of three parameters. The composition, thermal history, and data collection parameters are published in Reference 35 and the modal orientation relationship values are published in Reference 34 and listed in Table I. Here, ξ_1 is the smaller deviation from $\langle 110 \rangle$ -type Bain correspondence axis, ξ_2 is the large deviation from the $\langle 110 \rangle$ -type axis, and ξ_3 is the deviation from the $\langle 001 \rangle$ -type axis. This resulted in 24 crystallographic variants, the same number attained with the KS orientation relationship. For convenience of comparison, the three NW and KS modal values and corresponding Bunge Euler angles for a single variant (V_1) are also listed in Table I.

Each of the resulting five orientations (the PAG and its four annealing twins) was then rotated by the 12 $\gamma \rightarrow \alpha'$ variant rotations for the NW OR, the 24 $\gamma \rightarrow \alpha'$ rotations of the KS OR, or the 24 rotations of an experimentally measured (irrational) orientation relationship. This produced a total of 7260 post-transformation orientations (inclusive of misorientations between identical variants) for the experimental and KS relationships and 1830 orientations for NW. The minimum-angle misorientations between each of these orientations was then calculated assuming either cubic or tetragonal symmetry elements (representing the as-transformed martensite and the tempered martensite ferritic microstructures, respectively). Duplicate

Table I. The ξ and Bunge Euler Angles for the First Variant for the KS, NW, and Experimental Orientation Relationships

Rotation	KS (Deg)	NW (Deg)	Exp (Deg)
ξ_1	5.26	0.00	3.30
ξ_2	10.30	9.74	8.50
ξ_3	10.53	9.74	8.90
ϕ_1	114.2	135.0	116.1
Φ	10.5	9.6	8.9
ϕ_3	204.2	180.0	200.3

misorientation operations were identified to produce the set of potentially observable boundary misorientations within a single-twinned PAG, and the unique misorientations were then numbered. Henceforth, we will refer to these boundary misorientations as “intersections.” We have chosen to represent the variant intersections by a misorientation angle about a specific crystallographic direction. The misorientation that results from a given variant–variant intersection is labeled in a composition table with the cell colored according to the misorientation angle. Additionally, the misorientation axis is plotted in an inverse pole figure. These tables and figures effectively display which misorientation will be observed upon the intersection of two variants.

The numbering of the variants has been conducted in the same manner as in Payton *et al.*^[32] where consecutive variants are grouped into subsets of six that are formed on the same $\{111\}_\gamma$ (*i.e.*, V_1 through V_6 would share one $\{111\}_\gamma \parallel \{011\}_\alpha$ relationship, V_7 through V_{12} would share a different $\{111\}_\gamma \parallel \{011\}_\alpha$ relationship, and so on). Additionally, successive variant pairs have the same Bain correspondence matrices (V_1 and V_2 , V_5 and V_6 , V_9 and V_{10} , *etc*). Likewise, the numbering of misorientations corresponds to the aforementioned sub-block (low-angle), block and packet boundaries, all differing types of intragranular variant–variant ($V_i - V_j$) interfaces. Misorientations will be denoted as Δg_i , where Δg_0 is an identity misorientation operator (identity rotation about an arbitrary or undefined axis to bring the two variants into coincidence with one another). Identity misorientations are the result of two equivalent variants from the same PAG sharing an interface. When applying the KS orientation relationship, some variants originating from annealing twins in the parent austenite are exactly the same orientation. This can result in no observed misorientation across a $\Sigma 3$ austenite twin boundary,^[36–39] as will be further analyzed in the present work. Additionally, misorientations labeled Δg_1 correspond to a sub-block boundary and block boundaries are distinguished by Δg_{2-4} . Misorientations Δg_{5-16} refer to packet boundaries, and the aforementioned misorientations all refer to intra-parent cases, where a variant formed from the PAG intersects with another variant that formed from the PAG. For misorientations Δg_{17+} , which involve twin variants, the $V_i - V_j$ interfaces are undefined packet boundaries.

III. RESULTS

A. Kurdjumov–Sachs Orientation Relationship With Cubic Symmetry

Given a single-parent austenite grain transformed to martensite, the composition table assuming the KS orientation relationship is displayed in Figure 1. The two axes in the table correspond to a particular variant, numbered according to Tables AI through AIII in the Appendix section, which details the unique misorientation relationships that exist between variants for certain cases (intra-parent, parent–twin, and twin–twin).

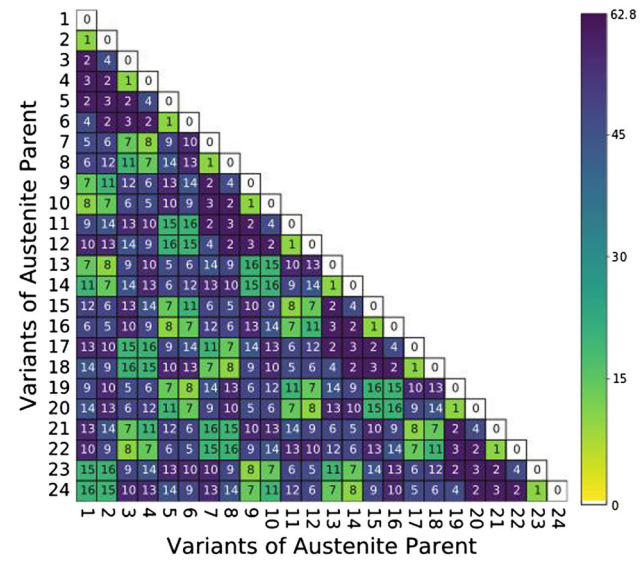


Fig. 1—Composition table exhibiting the possible variant–variant misorientations for prior intra-parent austenite grains.

Figure 1 covers the intra-parent case, where variants within a PAG intersect with variants within that same PAG. The plot itself is symmetric, so the top half mirrors the filled in bottom half of the plot. The identity misorientations ($V_i - V_i$) that occur between like variants are unobservable interfaces due to the lack of a misorientation and will later be found outside of the intra-parent case for the KS (and NW) orientation relationships.

The boxes in the table corresponding to the variant–variant misorientations are colored by the degree of misorientation, from light to dark, according to the corresponding colorbar. For cubic systems, the maximum misorientation angle is 62.8 deg.^[40] The majority of the misorientation squares are dark, meaning the misorientation angle is large for most of the variant intersections. Referring to Table AI, four of the possible 16 misorientations have angles near 60 deg, within 10 pct of the maximum possible cubic value, and there exist only 16 misorientations that occur from variant intersections out of 276 possibilities for the KS orientation relationship (excluding the $V_i - V_i$ and symmetric cases). However, it is also known that the austenite grains may contain FCC annealing twins before the phase transformation to martensite occurs,^[41] which would result in twin-related variants. Thus, it is necessary to determine what unique misorientations—if any—would result with the intersection of a parent austenite variant and a twinned austenite variant.

For sake of space and redundancy, only one parent–twin interaction will be presented since the results for all four produce identical sets of misorientations (although the misorientations appear in different locations within the composition table). The full composition tables for each specific case are available as supplemental data to the present paper in Figures S1–S9. The parent–60 deg [1 1 1] twin composition table can be found in Figure 2, with corresponding misorientation keys in Table AII.

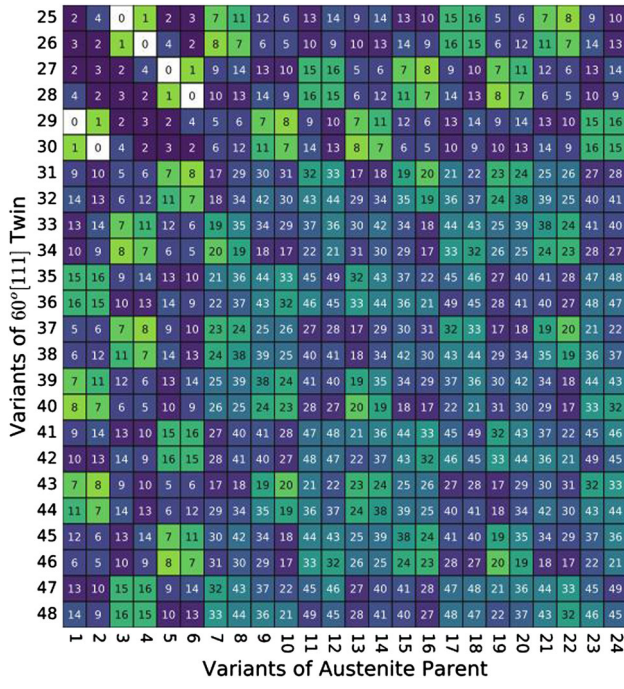


Fig. 2—The possible variant–variant misorientations for prior parent–60 deg $[1\bar{1}1]$ twin austenite grains.

As shown in Figure 2, the parent–twin interactions introduce considerably more misorientations than the intra-parent case alone, with 49 in total being observed. Additionally, the 16 misorientations found within the intra-parent case are repeated in the parent–twin cases, leaving 33 unique misorientations that would indicate the presence of at least one twin within the parent austenite grain. Again, we can see that the intersection squares all tend to be darker, indicative of higher misorientation angles, especially with regards to the unique parent–twin misorientations. The existence of six identity misorientations, consistent for each respective twinning case, results in the possibility of no observable interface within the transformed microstructure where an annealing twin boundary once existed for the KS orientation relationship.

Although rarer than $\Sigma 3$ annealing twins, it is possible for twin–twin variant intersections ($\Sigma 9$ boundaries^[42]) to occur in the parent austenite microstructure. This would consist of the intersection of two variants that transformed from austenite twins of differing rotations that nucleated within the same parent austenite grain, *i.e.*, the former boundary between two different twins of the same parent austenite. Composition tables were constructed for these interactions, with the composition table for the intersections between 60 deg $[\bar{1}\bar{1}1]$ and 60 deg $[1\bar{1}1]$ twins from the same austenite grain shown in Figure 3. The corresponding list of misorientation angle–axis pairs can be found in Table AIII. The same misorientations result from all other twin–twin composition tables; the complete set of tables is available in the supplemental material as Figures S1–S3.

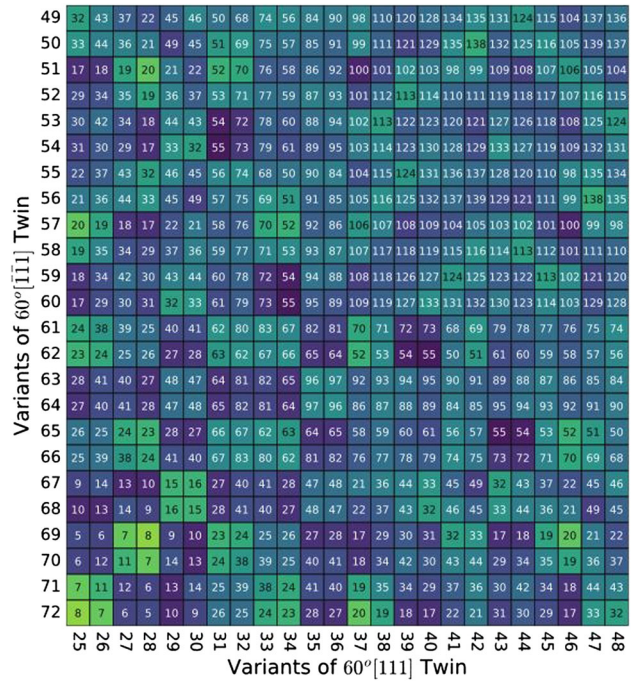


Fig. 3—Composition table exhibiting the possible variant–variant misorientations for differing twins that nucleated from the same parent austenite grain.

The twin–twin case includes misorientations Δg_5 to Δg_{139} , indicating a large number of the misorientations found with the intra-parent and parent–twin cases will also appear in twin–twin variant intersections. Additionally, we see that no identity misorientations exist in the twin–twin cases. The twin–twin intersections bring about 90 unique misorientations that can only be observed in twin–twin intersections, and are thus indicative of a prior $\Sigma 9$ boundary.

The existence of misorientations numbered above 16 would necessitate that at least one of the variants being observed came from an austenite twin. Twin variants of the same rotation intersecting with each other (for example, the composition table of 60 deg $[\bar{1}\bar{1}1]$ and 60 deg $[\bar{1}\bar{1}1]$) produce the exact same composition table as shown in Figure 1. Since these cases are highly unlikely, it can be assumed that the observance of Δg_1 through Δg_4 would indicate that at least one of the variants would have had to have nucleated from a parent austenite grain. These tables can also be found in the supplemental material provided as Figure S2. Additionally, out of all possible misorientations, only three could be considered as low-angle Δg_1 (10.53 deg), Δg_7 (14.88 deg), and Δg_8 (10.53 deg). The minimum misorientation angles are Δg_1 and Δg_8 , both (10.53 deg), and the maximum misorientation angle is Δg_{55} (60.83 deg).

To better visualize the directional aspects of the misorientations with respect to cubic symmetry, the axes for the intra-parent, parent–twin, and twin–twin cases were plotted on stereographic triangles and displayed in Figure 4. Tables AI through AIII can be used to identify the misorientation angles corresponding to each

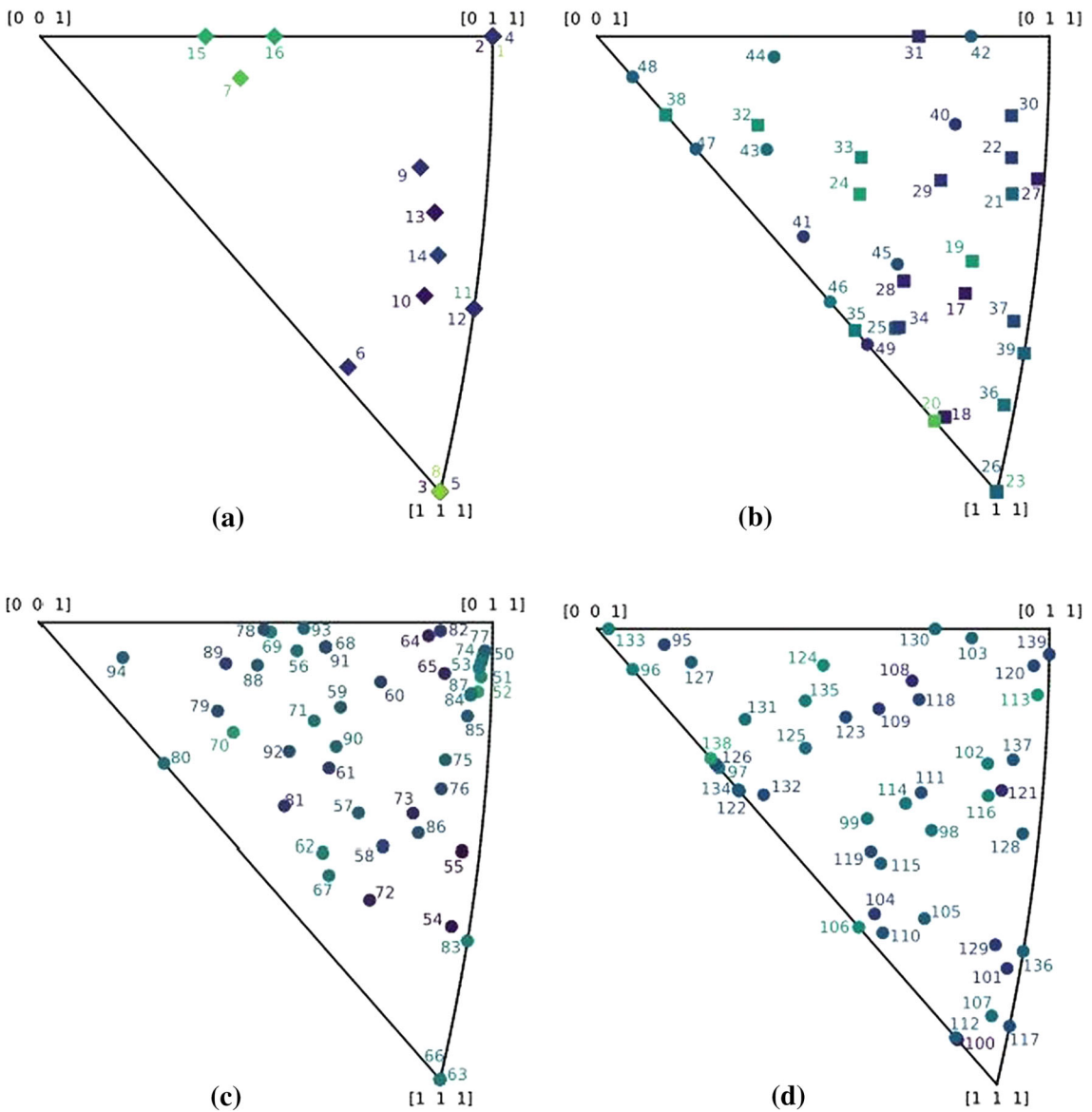


Fig. 4—Misorientation directional axes overlayed on stereographic triangles for the KS orientation relationship for (a) the intra-parent case, (b) the parent–twin case, and (c) and (d) the twin–twin case (split into two subfigures to reduce the density of points).

respective misorientation axis. Misorientation axes are colored according to misorientation angle using the same color key as used in Figure 1. Several misorientations are found to exhibit the same axes as one another. We can also see from the tables that some of the misorientation angles are very similar. This will be addressed in the Discussion section of this paper.

B. Nishiyama–Wassermann Orientation Relationship

NW has half of the number of variants as compared to KS due to the alignment of symmetry operators between parent and product phases. As such, V_1 and V_2 in the KS orientation relationship refer to V_1 in the NW orientation relationship, V_3 and V_4 in KS are V_2 in NW, and so on. Due to the reduced number of orientation

relationship variants, far fewer unique misorientations can be observed and a complete composition table exhibiting all of the possible variant combinations can be simultaneously represented in Figure 5.

The intra-parent case applying the NW orientation relationship involves five unique misorientations, while the parent–twin case has 15 misorientations and includes all of the intra-parent misorientations. Additionally, we can see the existence of three identity operators instead of six as in the KS case. Finally, in terms of the differing twin–twin variant intersections, there exist Δg_2 through Δg_{40} , excluding only Δg_1 . In comparing the tables for KS and NW, it is apparent that NW Δg_1 seems to combine KS Δg_2 – Δg_3 , in the process eliminating the existence of KS Δg_1 . As expected, the NW orientation relationship also results in almost all high

13	1	0	1	3	2	4	4	4	5	2	3	4	0																																											
14	1	1	0	4	4	5	2	3	4	3	2	4	1	0																																										
15	0	1	1	2	3	4	3	2	4	4	5	1	1	0																																										
16	4	2	3	6	12	13	6	7	8	9	10	11	2	3	4	0																																								
17	4	3	2	7	6	8	12	6	13	10	9	11	3	2	4	1	0																																							
18	5	4	4	8	13	14	13	8	14	11	11	15	4	4	5	1	1	0																																						
19	2	3	4	9	10	11	6	12	13	6	7	8	3	4	2	4	5	4	0																																					
20	3	2	4	10	9	11	7	6	8	12	6	13	2	4	3	2	4	3	1	0																																				
21	4	4	5	11	11	15	8	13	14	13	8	14	4	5	4	3	4	2	1	0																																				
22	3	4	2	6	7	8	9	10	11	6	12	13	4	2	3	4	2	3	4	5	4	0																																		
23	5	4	3	12	6	13	10	9	11	7	6	8	4	3	2	5	4	4	2	4	3	1	0																																	
24	4	5	13	8	14	11	15	8	13	14	13	8	14	5	4	4	4	3	2	3	4	2	1	0																																
25	14	13	8	15	11	11	8	14	13	4	5	4	13	8	14	16	19	25	29	35	39	37	32	40	0																															
26	8	6	7	11	10	9	6	13	12	3	4	2	6	7	8	17	20	26	30	31	29	34	33	32	1	0																														
27	13	12	6	11	9	10	7	8	6	2	4	3	12	6	13	18	21	27	31	36	35	38	34	37	1	0																														
28	14	8	13	14	8	13	11	15	11	5	4	4	8	13	14	19	16	25	32	37	40	35	29	39	2	3	4	0																												
29	8	7	6	13	6	12	10	11	9	4	3	2	7	6	8	20	17	26	33	34	32	31	30	29	3	2	4	1	0																											
30	13	6	12	8	7	6	9	11	10	4	2	3	6	12	13	21	18	27	34	38	37	36	31	35	4	5	1	0																												
31	9	10	13	12	6	6	8	7	2	3	4	9	10	11	22	24	23	17	18	16	21	20	19	3	4	2	5	4	0																											
32	15	11	11	14	13	8	13	14	8	4	4	5	11	11	15	23	23	28	26	27	25	27	26	25	2	4	3	2	1	0																										
33	11	10	9	8	6	7	12	13	6	3	2	4	10	9	11	24	22	23	20	21	19	18	17	16	4	5	4	3	2	1	0																									
34	5	4	4	4	3	2	3	4	2	1	0	1	4	5	11	11	15	8	13	14	13	8	14	4	2	3	4	5	4	0																										
35	4	2	3	4	2	3	4	5	4	0	1	1	2	3	4	9	10	11	6	12	13	6	7	8	4	3	2	5	4	4	0																									
36	4	3	2	5	4	4	2	4	3	1	0	1	3	2	4	10	9	11	7	6	8	12	6	13	5	4	4	4	3	2	1	0																								
37	6	8	7	10	11	9	4	3	2	13	6	12	8	7	6	33	34	32	31	30	29	20	17	26	35	36	31	27	18	21	34	37	38	12	13	6	0																			
38	13	14	8	11	15	11	5	4	4	14	8	13	14	8	13	32	37	40	35	29	39	19	25	25	16	19	32	40	37	13	14	8	1	0																						
39	12	13	6	9	11	10	4	2	3	8	7	6	13	6	12	34	38	37	36	31	21	15	21	27	31	30	26	17	20	33	32	34	6	8	7	1	0																			
40	7	8	6	6	13	12	3	4	2	11	10	9	8	6	7	30	31	29	34	33	32	17	20	26	16	18	17	23	22	24	20	19	21	9	11	10	2	3	4	0																
41	8	14	13	8	14	13	4	5	4	35	11	11	14	13	8	29	35	39	37	32	40	16	19	25	25	27	26	28	23	23	26	25	27	11	15	11	3	2	4	1	0															
42	6	13	12	7	8	6	2	4	3	11	9	10	13	12	6	31	36	35	38	34	37	18	21	27	19	21	20	23	24	22	17	16	18	10	11	9	4	4	5	1	0															
43	2	4	3	2	4	3	1	0	1	0	5	4	4	3	2	7	6	1	8	12	6	13	10	9	11	14	13	8	15	11	11	8	14	13	4	5	4	0																		
44	4	5	4	3	4	2	1	1	0	4	3	2	5	4	4	8	13	14	13	8	14	11	11	15	13	12	6	11	9	10	7	8	6	2	4	3	2	4	3	1	0															
45	3	4	2	4	5	4	0	1	1	4	2	3	4	2	3	6	12	13	6	7	8	9	10	11	8	6	7	11	10	9	6	13	12	3	4	2	4	5	4	0																
46	11	15	11	13	14	8	4	5	4	14	13	8	15	11	12	26	27	25	26	25	23	23	28	40	37	32	25	19	26	29	35	8	14	13	4	2	3	4	2	3	4	5	4	0												
47	9	11	10	12	13	6	3	2	4	8	6	7	6	11	10	9	20	21	19	18	17	16	24	22	23	32	34	33	26	20	17	30	29	31	7	8	6	4	3	2	5	4	4	2	4	3	1	0								
48	10	11	9	6	8	7	2	3	4	13	12	6	11	9	10	17	18	16	21	20	19	22	24	23	37	38	34	27	21	18	31	35	36	6	13	12	5	4	4	4	3	2	3	4	2	1	0									
49	6	12	13	4	2	3	8	7	6	9	11	10	12	13	6	36	31	35	21	18	27	34	38	37	33	23	24	22	19	21	20	18	17	16	17	10	9	11	17	16	17	10	9	11	17	26	20	31	29	30	7	6	8	32	34	33
50	7	6	8	4	3	2	13	6	12	10	11	9	6	8	7	31	30	29	20	17	26	33	34	32	23	22	14	16	18	17	21	19	20	9	10	11	18	17	27	21	36	35	31	6	12	13	37	38	34							
51	8	13	14	5	4	4	14	8	13	11	15	11	13	14	8	35	29	39	19	16	25	32	37	40	28	23	25	27	26	27	26	25	26	11	11	15	16	25	19	35	39	29	8	13	14	30	37	32								
52	3	2	4	1	0	1	5	4	4	2	4	3	2	4	3	12	6	13	10	9	11	7	6	8	11	10	9	8	6	7	12	13	6	3	2	4	11	15	11	13	14	8	4	4	5	14	13	8								
53	4	4	5	1	0	1	4	3	2	3	4	2	4	5	4	13	8	14	11	15	11	14	11	14	13	8	13	14	8	14	11	9	10	13	12	6	8	7	4	9	11	10	12	13	6	3	2	4	8	6	7					
54	2	3	4	0	1	1	4	2	3	4	5	4	3	4	2	6	7	8	9	10	11	6	12	13	15	15	11	14	13	8	13	14	8	4	5	10	11	9	6	8	7	2	3	4	13	12	6									
55	11	11	15	4	4	5	14	13	8	13	14	8	11	15	11	27	26	25	23	23	28	26	27	25	25	19	16	40	37	32	35	29	29	8	13	14	19	35	29	28	39	29	8	13	14	30	37	32								
56	10	9	11	3	2	4	8	6	7	12	13	6	9	11	10	18	17	16	24	22	23	20	21	19	27	21	18	37	38	34	36	35	31	6	12	13	20	26	17	34	32	33	6	7	8	29	31	30								
57	9	10	11	2	3	4	13	12	6	8	7	10	11	9	21	20	19	22	24	23	17	18	16	26	20	17	32	34	33	31	29	30	7	6	8	21	27	18	38	37	34	12	6	13	35	36	31									
58	6	7	8	3	4	2	11	10	9	6	13	12	7	8	6	34	33	32	37	20	26	30	11	29	27	18	21	35	36	31	38	37	34	12	6	13	22	23	24	18	16	17	10	9	11	19	21	20								
59	13	8	14	4	5	4	15	11	11	8	14	13	8	14	13	37	32	40	16	19	25	29	35	25	16	19	39	35	29	37	40	32	13	8	14	23	28	23	27	25	26	11	11	15	25	27	26									
60	12	6	13	2	4	3	11	9	10	7	8	6	6	13	12	38	34	37	18	21	27	31	36	35	26	37	20	29	31	30	34	32	33	6	7	8	24	23	22	21	19															

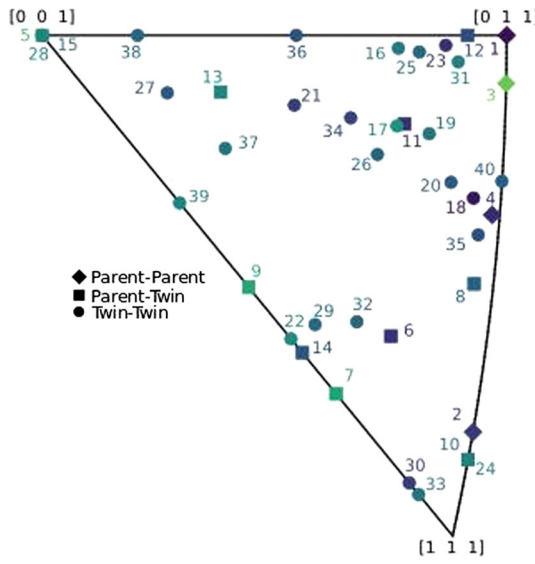


Fig. 6—Stereographic triangle plotting all misorientation axes with colored points corresponding to degree of misorientation angle for the NW orientation relationship.

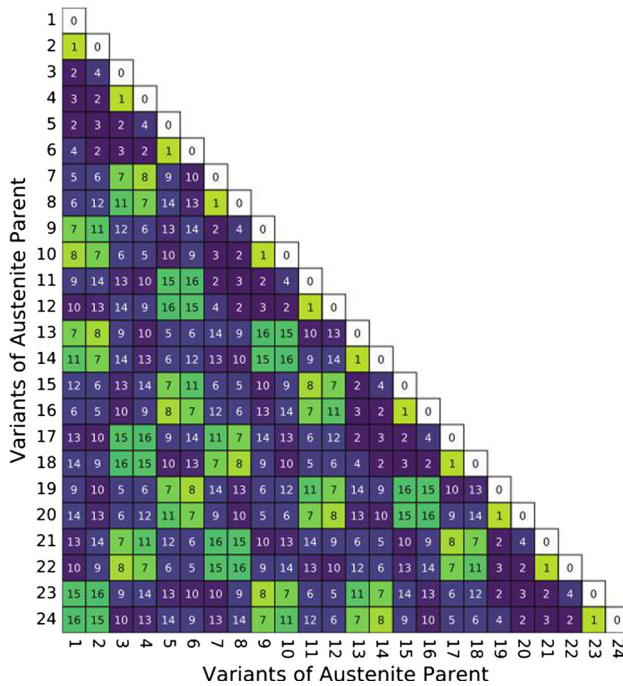


Fig. 7—Composition table exhibiting intra-parent variant intersections given an experimentally determined orientation relationship.

unique to the parent–twin case. In comparison, all sixteen misorientation operators in KS are shared between the parent and the twin.

The twin–twin composition table for the 60 deg [111]-60 deg $\bar{[1}\bar{1}1]$ twins using the experimental orientation relationship is given in Figure 9. The remaining composition tables can be found in the supplemental

	1	2	3	4	5	6	7	8	9	10	11	12	13	14	15	16	17	18	19	20	21	22	23	24
1	4	18	19	20	4	17	33	34	35	36	37	38	21	22	23	24	25	26	27	28	29	30	31	32
2	17	4	20	19	18	4	30	29	28	27	32	31	24	23	22	21	26	25	36	35	34	33	38	37
3	4	17	4	18	19	20	21	22	23	24	25	26	27	28	29	30	31	32	33	34	35	36	37	38
4	18	4	17	4	20	19	24	23	22	21	26	25	36	35	34	33	38	37	30	29	28	27	32	31
5	19	20	4	17	4	18	27	28	29	30	31	32	33	34	35	36	37	38	21	22	23	24	25	26
6	20	19	18	4	17	4	36	35	34	33	38	37	30	29	28	27	32	31	24	23	22	21	26	25
7	21	24	27	36	33	30	39	51	52	53	54	55	39	40	41	42	43	44	45	46	47	48	49	50
8	22	23	28	35	34	32	40	56	64	52	65	66	51	56	57	41	58	59	46	60	61	47	62	63
9	23	22	29	34	35	28	41	57	56	51	59	58	52	64	56	40	66	65	47	61	60	46	63	62
10	24	21	30	33	36	27	41	40	39	44	43	53	52	51	39	55	54	48	47	46	45	50	49	51
11	25	26	31	38	37	32	43	58	66	55	67	71	54	65	59	44	67	68	49	62	63	50	69	72
12	26	25	32	37	38	31	44	59	65	54	68	67	55	66	58	43	71	67	50	63	62	49	72	69
13	27	36	33	30	21	24	45	46	47	48	49	50	39	51	52	53	54	55	39	40	41	42	43	44
14	28	35	34	29	22	23	46	60	61	47	62	63	40	56	52	57	41	58	59	55	54	56	57	58
15	29	34	35	28	23	22	47	61	60	46	63	62	41	57	56	51	59	58	52	64	56	40	66	65
16	30	33	36	27	24	21	48	47	46	45	50	49	42	41	40	39	44	43	53	52	51	39	55	54
17	31	38	37	32	25	26	49	62	63	50	69	72	43	58	66	55	67	71	54	65	59	44	67	68
18	32	37	38	31	26	25	50	63	62	49	70	69	44	59	65	54	68	67	55	66	58	43	71	67
19	33	30	21	24	27	36	39	40	41	42	43	44	45	46	47	48	49	50	39	51	52	53	54	55
20	34	29	22	23	28	35	51	56	57	41	58	59	46	60	61	47	62	63	40	56	64	52	65	66
21	35	28	23	22	29	34	52	64	56	40	66	65	47	61	60	46	63	62	41	57	56	51	59	58
22	36	27	24	21	30	33	53	52	51	39	55	54	48	47	46	45	50	49	42	41	40	39	44	43
23	37	32	25	26	31	38	54	65	59	44	67	68	49	62	63	50	69	70	43	58	66	55	67	71
24	38	31	26	25	32	37	55	66	58	43	71	67	50	63	62	49	70	69	44	59	65	54	68	67

Fig. 8—Composition table displaying parent–twin variant intersections given an experimentally determined orientation relationship.

	1	2	3	4	5	6	7	8	9	10	11	12	13	14	15	16	17	18	19	20	21	22	23	24
1	4	96	102	78	118	124	138	156	162	144	172	178	186	198	208	216	222	223	219	212	203	192	225	224
2	73	97	103	79	119	125	139	157	163	145	173	179	187	199	209	217	223	226	220	213	204	193	227	225
3	74	98	104	80	120	126	140	158	164	146	174	180	188	189	190	191	186	187	197	196	195	194	193	192
4	75	99	105	81	121	127	141	159	165	147	175	181	189	200	201	202	198	199	207	206	205	195	204	203
5	76	100	106	82	122	128	142	160	166	148	176	182	190	201	210	211	208	209	215	214	206	196	213	212
6	77	101	107	83	123	129	143	161	167	149	177	183	191	202	211	218	216	217	221	215	207	197	220	219
7	78	102	96	4	124	118	144	162	156	138	178	172	192	203	212	219	224	225	216	208	198	216	222	223
8	79	103	97	73	125	119	145	163	157	139	179	173	193	204	213	220	225	227	227	217	209	198	226	223
9	80	104	98	74	126	120	146	164	158	140	180	174	194	195	196	197	192	193	191	190	189	188	187	186
10	81	105	99	75	127	121	147	165	159	141	181	175	195	205	206	207	203	204	202	201	200	189	199	198
11	82	106	100	76	128	122	148	166	160	142	182	176	196	206	214	215	212	213	211	210	201	199	208	207
12	83	107	101	77	129	123	149	167	161	143	183	177	197	207	215	221	219	220	218	211	201	191	217	216
13	84	108	113	89	130	135	150	168	171	155	170	169	158	159	160	161	156	157	167	166	165	164	163	162
14	85	109	112	88	131	134	151	160	155	151	153	152	140	141	142	143	138	139	149	148	147	146	145	144
15	86	110	111	87	132	133	152	169	170	153	184	185	180	181	182	183	178	179	177	176	175	174	173	172
16	87	111	110	86	133	132	153	170	169	152	185	184	174	175	176	177	172	173	183	182	181	180	179	178
17	88	112	109	85	134	131	154	165	150	151	152	153	146	147	148	149	144	145	143	142	141	140	139	138
18	89	113	108	84	135	130	155	171	168	150	169	170	164	165	166	167	162	163	161	160	159	158	157	156
19	90	114	115	91	136	137	131	130	135	134	133	132	120	121	122	123	118	119	129	128	127	126	125	124
20	91	115	114	92	137	136	134	135	130	131	132	123	127	128	129	124	125	123	122	121	120	119	118	117
21	92	93	94	95	90	91	85	84	89	88	87	86	74	75	76	77	4	73	83	82	81	80	79	78
22	93	94	95	96	91	92	88	87	84	85	86	87	80	81	82	83	78	79	77	76	75	74	73	4
23	94	95	96	97	92	93	90	89	88	84	85	86	87	80	81	82	83	78	79	77	76	75	74	73
24	95	94	93	92	91	90	88	87	84	85	86	87	80	81	82	83	78	79	77	76	75	74	73	4

Fig. 9—Composition table showing differing twin–twin variant intersections given an experimentally determined orientation relationship. The material provided as Figures S4-S7. Similar to the parent–twin case, several mis

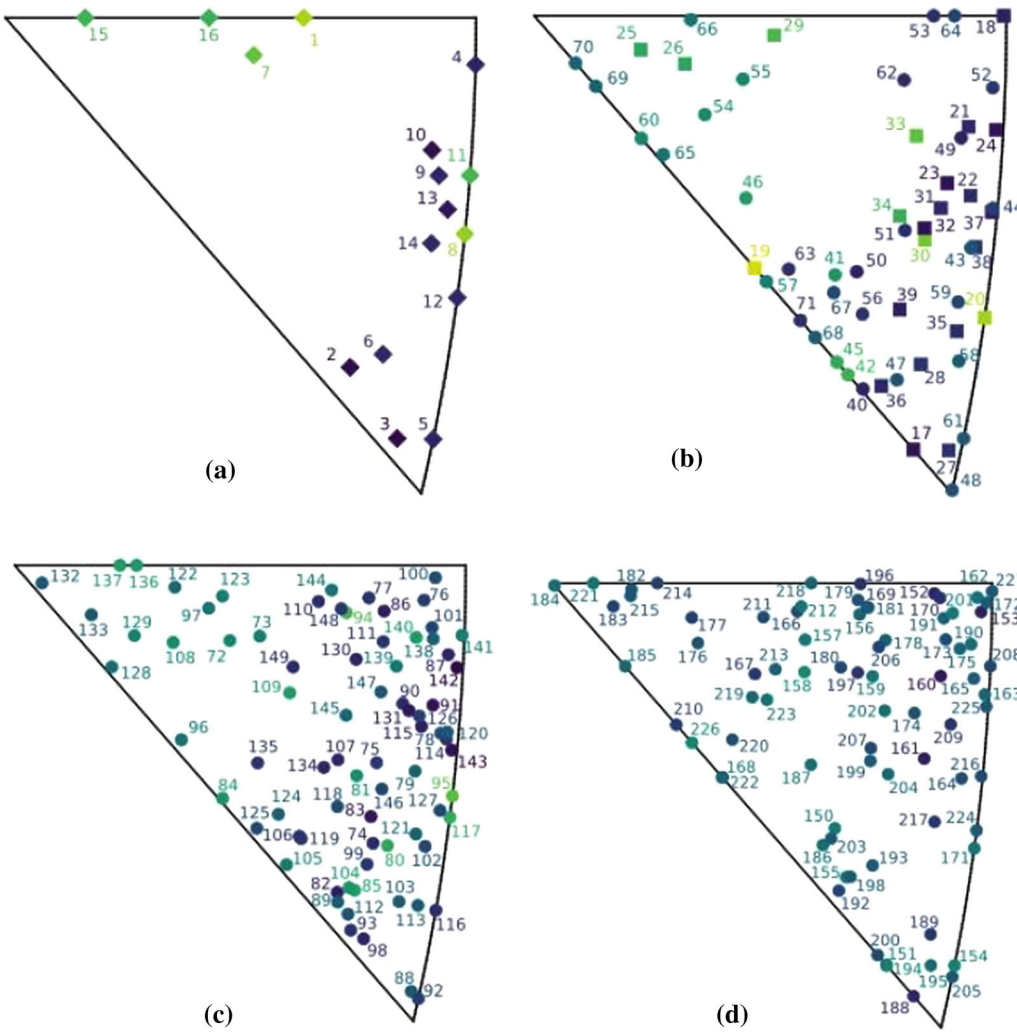


Fig. 10—Misorientation directional axes overlayed on stereographic triangles for the experimentally measured orientation relationship for: (a) the intra-parent case, (b) the parent-twin case, and (c) and (d) the twin-twin case (split into two subfigures to reduce density of points).

misorientation to exist in both the twin–twin case and the parent–twin or intra-parent cases is Δg_4 . All others are unique to the twin–twin case. There exist 156 unique misorientations for the twin–twin case, with a total of 227 misorientations for the experimental orientation relationship as a whole. This is significantly higher than the 139 misorientations found for the KS orientation relationship. Eight low-angle boundaries exist within the experimental orientation relationship. Three are at the same variant–variant intersection numbers as the KS case, meaning that they are produced from the same variant pairings: Δg_1 (6.60 deg), Δg_7 (12.58 deg), and Δg_8 (8.12 deg). There are five additional low-angle misorientations: Δg_{19} (3.19 deg), Δg_{20} (6.93 deg), Δg_{30} (11.15 deg), and Δg_{33} (13.14 deg) unique to the parent–twin case, and Δg_{95} (14.07 deg), unique to the twin–twin case.

Stereographic triangles of the misorientation axes corresponding to Figures 6 through 8 are given in Figure 10. It is clear from the figure that the experimentally observed orientation relationship tends to

produce several misorientations with rotation axes that are essentially parallel, where several of the points are very close to one another in the plot. The colors again relate to the degree of the misorientation by the same color scale as given in Figure 1, while the marker shapes indicate whether the Δg originates from the intra-parent, parent–twin, or twin–twin composition tables.

A pole figure containing the variant orientations for the three orientation relationships analyzed in Section III is displayed in Figure 11. In each case, the prior austenite orientation is aligned with the sample reference frame. The martensite variants of the parent austenite are indicated with black dots circumscribed by a colored circle indicating the hemisphere of the pole in stereographic projection. Each twin of the parent austenite orientation is represented by a different marker style according to the legend in the lower left. This figure concisely collects all of the variants so they can be easily compared, either within an orientation relationship to examine the differences between PAG and twin variants, or across orientation relationships to discover

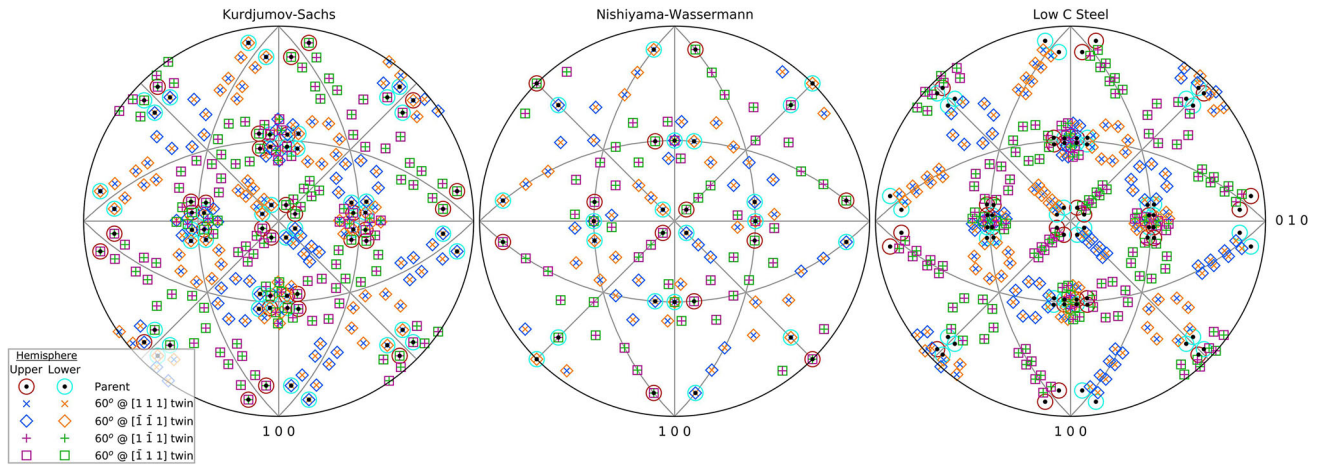


Fig. 11—Pole figures containing variant orientations for the three orientation relationships: KS (left), NW, and Experimental (right), all considering cubic symmetry.

disparities. Close examination of the pole figures reveals that the locations of intra-parent variants from KS and NW overlap with those of variants generated from Σ_3 twin boundaries, as has been reported elsewhere^[36–39], however, this overlap is not observed in the experimentally measured orientation relationship. Since all orientations are unambiguous, this increases the number of unique misorientations observed between the variants, as presented in Figures 7 through 9.

IV. KS ORIENTATION RELATIONSHIP CONSIDERING TETRAGONAL-BASED CRYSTAL SYMMETRY

As mentioned above, the previous cases analyzing $V_i - V_j$ intersections from an orientation relationship standpoint were all conducted using cubic symmetry. That is, the austenite \rightarrow martensite transformation was really an $fcc \rightarrow bcc$ phase transformation. To study whether product crystal structure affects misorientation data, tetragonal symmetry was applied to the variant rotation matrices in the calculation of the composition tables. This corresponds to the $fcc \rightarrow bct$ transformation. The KS orientation relationship was used to compare the effects of cubic and tetragonal symmetry on misorientation calculations. Furthermore, intra-parent, parent-twin, and twin-twin variant intersections were examined. The intra-parent composition table is given in Figure 12. The colormapping of the composition tables was comparable in style to the cubic case but was normalized to the maximum tetragonal misorientation angle of 98.42 deg^[40] rather than 62.3 deg for cubic systems, as indicated adjacent to the plot.

In Figure 12, we again see exactly the same misorientation locations within the composition table as both the cubic-KS and experimental case, with 16 misorientations in total. Overall, the tetragonal-based misorientation angles seem to fall further away from the maximum misorientation angle. Additionally, as seen in the cubic case, the same three numbered misorientations corresponding to the intra-parent case could be

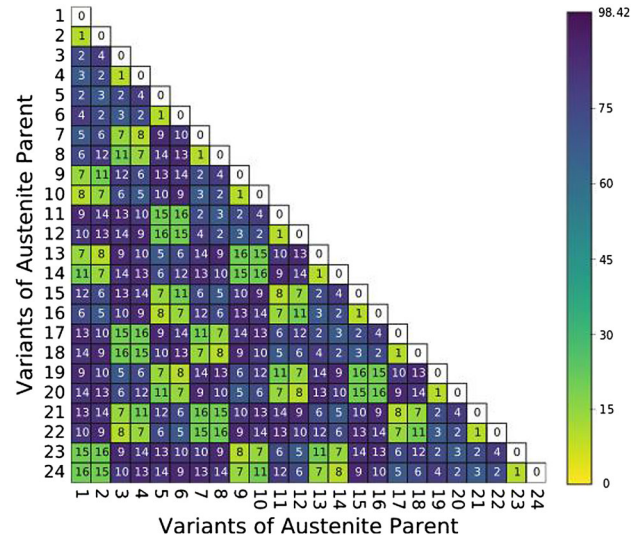


Fig. 12—Intra-parent composition table for tetragonal symmetry using KS orientation relationship.

classified as low-angle boundaries: Δg_1 (10.53 deg), Δg_7 (14.88 deg), and Δg_8 (10.53). It is interesting to note that all three of these misorientation numbers were low-angle boundaries across orientation relationship and cubic symmetry when considering 24 variants. All the rest of the misorientations correspond to high-angle boundaries.

When considering the parent-twin case for tetragonal symmetry for all four possible twin rotations, all of the misorientation angles are rather large, with none falling below 40 deg. Again, we see that there are no shared variants, but in this case, the location where the shared variants exist in the cubic-KS case (Section III) is not low-angle, coming in at 90.00 deg (Δ_3). Not only is this misorientation angle very far from an identity rotation, no misorientations from the intra-parent case overlap with the parent-twin case, ergo each misorientation is unique. A total of 55 unique misorientations exist,

25	17	19	20	21	17	18	34	35	36	37	38	39	22	23	24	25	26	27	28	29	30	31	32	33
26	18	17	21	20	19	17	31	30	29	28	33	32	25	24	23	22	27	26	37	36	35	34	39	38
27	17	18	17	19	20	21	22	23	24	25	26	27	28	29	30	31	32	33	34	35	36	37	38	39
28	19	17	18	17	21	20	25	24	23	22	27	26	37	36	35	34	39	38	31	30	29	28	33	32
29	20	21	17	18	17	19	28	29	30	31	32	33	34	35	36	37	38	39	22	23	24	25	26	27
30	21	20	19	17	18	17	37	36	35	34	39	38	31	30	29	28	33	32	25	24	23	22	27	26
31	22	25	28	37	34	31	40	52	53	54	55	56	40	41	42	43	44	45	46	47	48	49	50	51
32	23	24	29	36	35	30	41	57	65	53	66	67	52	57	58	42	59	60	47	61	62	48	63	64
33	24	23	30	35	36	29	42	58	57	52	60	59	53	65	57	41	67	66	48	62	61	47	64	63
34	25	22	31	34	37	28	43	42	41	40	45	44	54	53	52	40	56	55	49	48	47	46	51	50
35	26	27	32	39	38	33	44	59	67	56	68	72	55	66	60	45	68	69	50	63	64	51	70	71
36	27	26	33	38	39	32	45	60	66	55	69	68	56	67	59	44	72	68	51	64	63	50	71	70
37	28	37	34	31	22	25	46	47	48	49	50	41	52	53	54	55	56	40	41	42	43	44	45	
38	29	36	35	30	23	24	47	61	62	48	63	64	41	57	65	53	66	67	52	57	58	42	59	60
39	30	35	36	29	24	23	48	62	61	47	64	63	42	58	57	52	60	59	53	65	57	41	67	66
40	31	34	37	28	25	22	49	48	47	46	51	50	43	42	41	40	45	44	54	53	52	40	56	55
41	32	39	38	33	26	27	50	63	64	51	70	71	44	59	67	56	68	72	55	66	60	45	68	69
42	33	38	39	32	27	26	51	64	63	50	71	70	45	60	66	55	69	68	56	67	59	44	72	68
43	34	31	22	25	28	37	40	41	42	43	44	45	46	47	48	49	50	51	40	52	53	54	55	56
44	35	30	23	24	29	36	52	57	58	42	59	60	47	61	62	48	63	64	41	57	65	53	66	67
45	36	29	24	23	30	35	53	65	57	41	67	66	48	62	61	47	64	63	42	58	57	52	60	59
46	37	38	25	22	31	34	54	53	52	40	56	55	49	48	47	46	51	50	43	42	41	40	45	44
47	38	33	26	27	32	39	55	66	60	45	68	69	50	63	64	51	70	71	44	59	67	56	68	72
48	39	32	27	26	33	38	56	57	59	44	72	68	51	64	63	50	71	70	45	60	66	55	69	68

Variants of Austenite Parent

Variants of $60^\circ[111]$ Twin

49	73	97	103	79	119	125	139	157	163	145	173	179	187	199	209	217	223	224	220	213	204	193	226	225
50	74	98	104	80	120	126	140	158	164	146	174	180	188	200	210	218	224	227	221	214	205	194	228	226
51	75	99	105	81	121	127	141	159	165	147	175	181	189	190	191	192	187	188	198	197	196	195	194	193
52	76	100	106	82	122	128	142	160	166	148	176	182	190	201	202	203	199	200	208	207	206	196	205	204
53	77	101	107	83	123	129	143	161	167	149	177	183	191	202	211	212	209	210	216	215	207	197	214	213
54	78	102	108	84	124	130	144	162	168	150	178	184	192	203	212	219	217	218	222	216	208	198	221	220
55	79	103	97	73	125	119	145	163	157	139	179	173	193	204	213	220	225	226	217	209	199	227	223	
56	80	104	98	74	126	120	146	164	158	140	180	174	194	205	214	221	226	228	218	210	200	188	227	224
57	81	105	99	75	127	121	147	165	159	141	181	175	195	196	197	198	193	194	192	191	190	189	188	187
58	82	106	100	76	128	122	148	166	160	142	182	176	196	206	207	208	204	205	203	202	201	190	200	199
59	83	107	101	77	129	123	149	167	161	143	183	177	197	207	215	216	213	214	212	211	202	191	210	209
60	84	108	102	78	130	124	150	168	162	144	184	178	198	208	202	222	220	221	219	212	203	192	218	217
61	85	109	114	90	131	136	151	169	172	156	171	170	159	160	161	162	157	158	168	167	166	165	164	163
62	86	110	113	89	132	135	152	151	156	155	154	153	141	142	143	144	139	140	150	149	148	147	146	145
63	87	111	112	88	133	134	153	170	171	154	185	186	181	182	183	184	179	180	178	177	176	175	174	173
64	88	112	111	87	134	133	154	171	170	153	186	185	175	176	177	178	173	174	184	183	182	181	180	179
65	89	113	110	86	135	132	155	156	151	152	153	154	147	148	149	150	145	146	144	143	142	141	140	139
66	90	114	109	85	136	131	156	172	169	151	170	171	165	166	167	168	163	164	162	161	160	159	158	157
67	91	115	116	92	137	138	132	131	136	135	134	138	121	122	123	124	119	120	130	129	128	127	126	125
68	92	116	115	91	138	137	135	136	131	132	133	134	127	128	129	130	125	126	124	123	122	121	120	119
69	93	94	95	96	91	92	86	85	90	89	88	87	75	76	77	78	73	74	84	83	82	81	80	79
70	94	117	118	95	115	116	110	109	114	113	112	111	99	100	101	102	97	98	108	107	106	105	104	103
71	95	118	117	94	116	115	113	114	110	111	112	105	106	107	108	103	104	102	101	100	99	98	97	96
72	96	95	94	93	92	91	89	90	85	86	87	88	81	82	83	84	79	80	78	77	76	75	74	73

Variants of $60^\circ[111]$ Twin

Experimental error in orientation measurement with EBSD will result in some misorientations being indistinguishable from one another. Bingham *et al.*^[43] found that 99 pct of intragranular orientation measurements within a well-annealed grain structure fell within 0.91 deg of one another. Taking 1 deg as a conservative estimate of the angular resolution tolerance for EBSD, it is found in our results that the cubic-KS orientation relationship would give three indistinguishable misorientations, as given in Table EXI. Two exist in the twin-twin case ($\Delta g_{50}-\Delta g_{77}$, $\Delta g_{84}-\Delta g_{87}$) and one ($\Delta g_{39}-\Delta g_{136}$) exists in both the parent-twin and the twin-twin tables. The tetragonal KS would give four indistinguishable misorientation operators, where again one misorientation could be misinterpreted within the parent-twin case and the twin-twin case ($\Delta g_{62}-\Delta g_{225}$) and three could be misidentified within twin-twin interaction ($\Delta g_{139}-\Delta g_{166}$, $\Delta g_{142}-\Delta g_{163}$, $\Delta g_{173}-\Delta g_{176}$). Finally, our investigated experimental orientation relationship would give three possible indistinguishable misorientations, where two overlap between the parent-twin and the twin-twin case ($\Delta g_{59}-\Delta g_{102}$, $\Delta g_{61}-\Delta g_{205}$) and one within only the twin-twin case ($\Delta g_{147}-\Delta g_{174}$). Cubic NW would give zero indistinguishable misorientation operators.

This observation could be significant for a number of reasons. When considering Table EXI, some of the possible indistinguishable misorientations stem from variant intersections of $\Sigma 3$ twins in the parent grain, while others stem from variant intersections of former $\Sigma 9$ twins, with none being specific to the intra-parent case. Experimentally, it may be difficult to distinguish between $\Sigma 3$ and $\Sigma 9$ boundaries if some of the misorientation angle-axis pairings are so similar to each other. In terms of austenite

reconstruction codes, this could possibly result in misclassifications of certain variant–variant intersections and thus suggest a parent–twin boundary segment where a twin–twin boundary segment should exist (or vice-versa). It is also worth noting that the scatter in crystallographic orientations for any given variant within the prior austenite grain is typically significantly larger than the experimental error in EBSD.^[34]

The repetition of misorientation operators between the intra-parent and parent–twin composition tables may have a significant impact on possible austenite reconstructions, because it means the position of the boundary itself is ambiguous in the cubic-KS orientation relationship. Furthermore, for the parent–twin case, the cubic-KS orientation relationship results in an (unobservable) identity misorientation. This would manifest itself in the transformed microstructure as the former twin boundary appearing discontinuous. Abbasi *et al.*^[36] attributed the apparent discontinuities at parent austenite $\Sigma 3$ boundaries to a prevalence of these identity operator variants at the twin interface, and justified their variant selection through an energy minimization argument. Shared variants between parent and twin minimize interfacial energy, effectively resulting in a higher-probabilistic choice of these variants forming at prior austenite $\Sigma 3$ grain boundaries. Our “KS-like” experimentally determined orientation relationship delivers a misorientation for variant pairs where one is not observed for KS, but at ~ 3.2 deg, it is smaller than a typical threshold for boundary identification in EBSD. The low misorientation angle may result in a minimized interfacial energy between these variants while remaining consistent with the ambiguous $\Sigma 3$ grain boundaries characterized by EBSD.

Although not shown in the present work, analysis of several other experimental orientation relationships resulted in similar misorientation distributions with varying misorientation angle–axis pairings. This paper compared the KS and experimental KS-like orientation relationships to show that specific orientation relationships must be applied to differing samples of steel if an accurate analysis of the material is to be constructed. For example, the KS misorientation ΔG_1 has an angle axis pairing of 10.53 deg @ $\langle 110 \rangle$, whereas the experimental orientation relationship misorientation ΔG_1 exhibits an angle axis pairing of 6.59 deg @ $\langle 047 \rangle$. Thus, it is clear that the sub-block boundary is substantially different between KS and the experimentally observed orientation relationship, even though the latter is similar to the rational KS orientation relationship. If a separate orientation relationship is used that differs vastly from the KS orientation relationship, it can be assumed that the observable misorientations will differ even more. This would suggest a substantial impact on the accuracy and efficacy of reconstructed austenite microstructures when disparate steel samples are being analyzed. The present work illustrates the potential importance of measuring the orientation relationship in each alloy for reconstruction, since the actual (irrational) misorientations between variants can be significantly different from those in the KS or NW orientation relationships.

Not only does the orientation relationship itself have a considerable impact on the possible misorientations that can exist between variants generated from an austenite grain, but symmetry plays a major role as well. It is known that we cannot measure the actual orientation when assuming a tetragonal structure due to pseudosymmetry, and as such the common practice is to assume cubic symmetry and neglect any tetragonal c-axis distortion. However, the present work demonstrates that differences exist between the sets of misorientation operators one would expect for the KS orientation relationship when the crystal symmetry is tetragonal as opposed to cubic. First, the latter produces significantly more misorientations than the cubic case (228 compared with 139, respectively). Furthermore, the tetragonal case does not produce any identity misorientations between the parent–twin case, as does the cubic case. In fact, the parent–twin table for tetragonal symmetry does not produce a misorientation angle < 50.0 deg, whereas the cubic case contains eight unique cases where the misorientation angle is < 30 deg, including the case where no misorientation angle exists. The variants that generate identity misorientations in the cubic-KS case produce misorientation angles of 90 deg when tetragonality is considered (see Table DIX in Appendix D, Δg_{20}). This would suggest that variants adjacent to austenite twin boundaries should not overlap with parent boundaries. In fact, they should be easily distinguishable for austenite reconstruction codes if an advancement in EBSD indexing technique enabled unambiguous definition of the martensite crystal orientation through identification of the tetragonal c-axis.^[44] Since practical limitations of camera and Hough transform resolution result in better indexing using cubic symmetry, until the time that such a characterization advancement is realized, it may be the case that austenite reconstructions exhibit larger errors with increasing carbon content (tetragonality).

VI. CONCLUSIONS

Both orientation relationship and martensite crystal structure significantly affect possible martensite variant intersections, introducing varying numbers of misorientations and degrees of misorientation. Furthermore, inclusion of prior austenite twins increases the total number of possible misorientations between intersecting variants. From the present work, the following conclusions were drawn:

- (1) If the KS or NW orientation relationships were exactly exhibited in a material, then the prior location of an austenite annealing twin boundary would be ambiguous on observation of the product martensite phase due to the presence of identity operators and intra-parent misorientation operators.
- (2) Although experimentally observed orientation relationships in Fe alloys are irrational, the number of misorientations exhibited within a single prior austenite orientation are the same as the KS case (16).

- (3) The presence of certain characteristic misorientations can be indicative of the presence of a $\Sigma 3$ or $\Sigma 9$ boundary in a prior austenite grain; however, the large number of these possible characteristic misorientations and their similarity to other misorientations that could be exhibited within a single prior austenite grain present a challenge in uniquely identifying the location of the boundaries related to prior austenite annealing twins.

The results presented here may be useful in austenite reconstruction, as they provide constraints on how an austenite grain could have transformed given the observable martensite.

ACKNOWLEDGMENTS

AFB and SRN received support from the Air Force Office of Scientific Research (AFOSR) Summer Faculty Fellowship Program (SFFP) for the portion of this work performed at the Materials and Manufacturing Directorate of the Air Force Research Laboratory (AFRL/RX) and from the Dayton Area Graduate Studies Institute (DAGSI) for the portion of the work performed at Ohio State University. EJP was supported by the Deutsche Forschungsgemeinschaft (DFG) for the portion of this work completed at the Federal Institute for Materials Research and Testing (BAM) in Berlin (Grant PA 2285/1-1) and by the Metallic Materials and Processes Research Team for the portion performed at AFRL/RX. VAY was supported under DFG Grant YA 326/2-1 for the portion of the work performed at Ruhr-Universität Bochum.

APPENDIX

For Tables AI through DX below, which list the complete misorientation list for the analyzed cases, a few of the notations may be new to the reader and as such will be described here briefly. Consistent with the text, Δg_i refers to a specific misorientation resulting from the variant–variant interactions. The term $\theta(\Delta g_i)$ refers to the misorientation angle, always measured in degrees, while the term $\vec{r} \equiv [r_1, r_2, r_3]$ is the approximate low-index axis of rotation for the misorientation. The term $\delta(\Delta g_i)$ is the deviation of the true axis from the true axis from the approximate low-index axis of rotation. Finally, the concluding table—Table EXI—is the comparison of similar misorientations that fall within 1 deg of each other. In regards to notation, the differing misorientations are denoted by the subscripts (i,j) such that $\Delta\theta(\Delta g_{i,j})$ would represent the angular difference between misorientation angles $\theta(\Delta g_i)$ and $\theta(\Delta g_j)$. Additionally, $\Delta\vec{r}(\Delta g_{i,j})$ would represent the angular difference between misorientation axes r_i and r_j .

APPENDIX A: KS-CUBIC ORIENTATION RELATIONSHIP MISORIENTATION DATA

See Tables AI, AII, AIII.

Table AI. Intra-parent Misorientation List for KS Orientation Relationship Considering Cubic Symmetry

Δg_i	$\theta(\Delta g_i)$ (deg)	\vec{r}	$\delta(\Delta g_i)$ (deg)
0	0.00	[0 0 1]	0.00
1	10.53	[0 1 1]	0.25
2	60.00	[0 1 1]	0.25
3	60.00	[1 1 1]	0.00
4	49.27	[0 1 1]	0.25
5	49.27	[1 1 1]	0.00
6	50.42	[2 2 3]	1.39
7	14.90	[1 3 8]	2.93
8	10.53	[1 1 1]	0.00
9	50.51	[1 4 5]	1.89
10	57.21	[3 5 6]	0.28
11	20.60	[3 5 5]	1.79
12	51.73	[3 5 5]	1.79
13	57.21	[2 5 6]	0.73
14	47.11	[2 4 5]	2.28
15	20.60	[0 1 3]	1.27
16	21.06	[0 3 7]	0.96

Table AII. Parent–Twin Misorientation List for KS Orientation Relationship Considering Cubic Symmetry

Δg_i	$\theta(\Delta g_i)$ (deg)	\vec{r}	$\delta(\Delta g_i)$ (deg)
17	55.61	[3 5 6]	1.05
18	54.84	[3 3 4]	1.33
19	25.00	[2 4 5]	0.99
20	15.45	[3 3 4]	0.63
21	37.24	[2 6 7]	1.60
22	47.56	[2 6 7]	2.78
23	21.06	[1 1 1]	0.00
24	23.51	[1 2 4]	1.45
25	40.28	[3 4 6]	2.35
26	38.94	[1 1 1]	0.00
27	55.23	[1 4 4]	1.34
28	53.51	[2 3 5]	2.26
29	49.19	[2 5 7]	1.27
30	45.80	[1 6 7]	1.20
31	51.32	[0 5 8]	0.74
32	26.11	[1 2 7]	0.70
33	29.12	[1 3 6]	2.27
34	47.56	[3 4 6]	2.10
35	33.57	[1 1 2]	1.71
36	34.85	[4 5 5]	1.15
37	44.35	[3 5 5]	1.45
38	28.41	[1 1 8]	0.00
39	38.94	[2 3 3]	0.76
40	49.19	[1 5 7]	1.22
41	47.83	[3 3 8]	2.17
42	40.28	[0 4 5]	0.92
43	34.85	[1 2 6]	1.33
44	35.45	[0 1 3]	1.81
45	43.00	[2 3 5]	0.48
46	33.57	[1 1 2]	1.71
47	40.28	[1 1 5]	1.35
48	38.94	[1 1 9]	3.65
49	51.80	[4 4 7]	0.00

Table AIII. Twin–Twin Misorientation List for KS Orientation Relationship Considering Cubic Symmetry

Δg_i	$\theta(\Delta g_i)$ (deg)	\vec{r}	$\delta(\Delta g_i)$ (deg)	Δg_i	$\theta(\Delta g_i)$ (deg)	\vec{r}	$\delta(\Delta g_i)$ (deg)
50	38.33	[0 1 1]	3.21	95	45.10	[0 1 8]	1.44
51	27.82	[1 6 6]	2.59	96	31.59	[1 1 9]	3.65
52	21.84	[1 6 6]	1.75	97	33.25	[2 2 9]	0.52
53	32.33	[1 6 6]	3.28	98	33.57	[1 2 3]	1.65
54	59.55	[3 5 5]	1.84	99	33.25	[2 3 6]	1.79
55	60.83	[1 2 2]	2.04	100	57.94	[5 5 6]	0.39
56	33.75	[0 1 2]	2.40	101	49.43	[3 4 4]	1.73
57	38.63	[1 2 3]	0.67	102	32.33	[2 6 7]	1.46
58	45.54	[3 5 7]	0.73	103	36.93	[0 4 5]	1.02
59	39.87	[1 4 7]	1.25	104	47.91	[4 4 7]	2.19
60	46.75	[1 5 7]	1.73	105	38.94	[4 5 7]	1.00
61	48.70	[2 4 7]	1.49	106	28.05	[4 4 7]	1.45
62	30.26	[2 3 5]	0.69	107	35.43	[4 5 5]	1.85
63	28.41	[1 1 1]	0.00	108	51.73	[1 5 8]	1.73
64	55.06	[0 4 5]	1.17	109	48.08	[1 4 7]	0.77
65	54.92	[1 6 7]	1.98	110	42.11	[4 4 7]	1.30
66	31.59	[1 1 1]	0.00	111	43.13	[1 2 3]	1.65
67	33.25	[3 4 7]	1.27	112	40.28	[5 5 6]	0.00
68	39.87	[0 4 7]	2.11	113	26.45	[1 6 6]	1.75
69	29.87	[0 3 7]	0.92	114	33.57	[1 2 3]	1.81
70	24.01	[1 2 5]	1.71	115	38.94	[3 4 7]	0.41
71	33.75	[1 3 6]	1.71	116	30.93	[2 5 6]	0.79
72	55.06	[3 4 6]	1.21	117	44.08	[4 5 5]	1.40
73	53.85	[2 4 5]	1.66	118	45.54	[1 5 8]	1.06
74	31.96	[0 1 1]	2.82	119	43.40	[3 4 7]	1.54
75	37.94	[2 6 7]	1.23	120	44.26	[0 1 1]	3.21
76	45.10	[2 6 7]	1.37	121	50.75	[2 6 7]	0.83
77	38.63	[0 1 1]	2.37	122	44.73	[2 2 7]	1.12
78	42.85	[0 2 5]	0.64	123	43.87	[1 3 6]	1.22
79	44.35	[1 2 6]	1.17	124	28.05	[0 3 7]	3.23
80	34.36	[2 2 9]	0.52	125	35.43	[1 2 5]	0.00
81	50.75	[2 3 6]	1.19	126	45.80	[2 2 9]	0.00
82	49.43	[0 6 7]	0.90	127	38.94	[0 1 6]	3.04
83	31.59	[2 3 3]	0.76	128	40.28	[2 5 5]	1.54
84	35.78	[1 6 7]	2.57	129	47.91	[2 3 3]	2.51
85	41.21	[1 5 5]	2.15	130	36.92	[0 2 3]	0.91
86	42.11	[2 4 5]	0.00	131	35.43	[1 2 6]	0.65
87	35.11	[1 6 7]	2.61	132	44.08	[2 2 7]	1.75
88	39.99	[1 3 8]	3.46	133	30.93	[0 0 1]	1.15
89	46.95	[1 3 8]	3.26	134	40.28	[1 1 4]	1.39
90	36.93	[1 3 5]	1.04	135	31.96	[1 3 8]	1.01
91	42.85	[0 4 7]	2.26	136	38.33	[2 3 3]	0.15
92	44.35	[1 2 4]	1.55	137	41.21	[2 6 7]	2.31
93	36.93	[0 1 2]	0.89	138	22.75	[2 2 9]	0.83
94	37.94	[0 1 7]	3.18	139	45.80	[0 1 1]	1.94

APPENDIX B: NW-CUBIC ORIENTATION RELATIONSHIP MISORIENTATION DATA

See Table BIV.

Table BIV. Misorientation List for NW Orientation Relationship with Cubic Symmetry

Δg_i	$\theta(\Delta g_i)$ (deg)	\vec{r}	$\delta(\Delta g_i)$ (deg)	Δg_i	$\theta(\Delta g_i)$ (deg)	\vec{r}	$\delta(\Delta g_i)$ (deg)
0	0.00	[0 0 1]	0.00	21	48.11	[1 4 8]	1.45
1	60.00	[0 1 1]	0.25	22	30.01	[1 1 2]	0.49
2	50.05	[3 4 4]	0.36	23	52.24	[0 5 6]	0.85
3	13.76	[1 6 6]	3.32	24	31.59	[5 6 6]	0.18
4	53.69	[1 3 3]	0.78	25	38.61	[0 3 4]	1.36
5	19.47	[0 0 1]	0.00	26	39.12	[1 4 6]	1.31
6	51.41	[2 3 4]	1.19	27	42.40	[1 2 9]	1.44
7	24.47	[3 3 5]	0.00	28	31.59	[0 0 1]	0.00

Table BIV. continued

Δg_i	$\theta(\Delta g_i)$ (deg)	\vec{r}	$\delta(\Delta g_i)$ (deg)	Δg_i	$\theta(\Delta g_i)$ (deg)	\vec{r}	$\delta(\Delta g_i)$ (deg)
8	40.66	[1 2 2]	2.34	29	37.58	[1 1 2]	2.37
9	23.12	[2 2 5]	0.27	30	49.12	[5 5 6]	0.00
10	38.94	[5 6 6]	0.18	31	31.70	[0 6 7]	1.97
11	52.63	[1 5 7]	0.65	32	38.94	[3 4 6]	1.18
12	45.38	[0 6 7]	0.86	33	35.43	[5 5 6]	1.07
13	30.75	[1 3 9]	1.44	34	46.72	[1 5 8]	1.24
14	42.69	[1 1 2]	1.15	35	45.38	[1 3 3]	2.05
15	38.94	[0 0 1]	0.00	36	43.37	[0 1 2]	1.04
16	33.56	[0 5 7]	0.88	37	35.43	[1 2 6]	0.58
17	27.47	[1 5 7]	0.00	38	38.94	[0 1 6]	0.26
18	58.94	[1 3 3]	2.74	39	31.48	[1 1 4]	0.61
19	34.92	[1 5 6]	1.53	40	41.08	[1 4 4]	0.43
20	41.76	[2 6 7]	1.34				

**APPENDIX C: EXPERIMENTAL-CUBIC
ORIENTATION RELATIONSHIP
MISORIENTATION DATA**

See Tables CV, CVI, CVII.

Table CV. Intra-parent Misorientation List for Experimental Orientation Relationship Considering Cubic Symmetry

Δg_i	$\theta(\Delta g_i)$ (deg)	\vec{r}	$\delta(\Delta g_i)$ (deg)
0	0.00	[0 0 1]	0.00
1	6.60	[0 4 7]	0.36
2	59.48	[2 2 3]	2.56
3	60.14	[5 5 6]	1.73
4	53.70	[1 6 6]	3.16
5	52.51	[4 5 5]	1.94
6	51.85	[3 4 5]	0.95
7	12.58	[0 3 7]	3.47
8	8.12	[2 5 5]	0.77
9	52.31	[2 6 7]	1.64
10	58.63	[2 6 7]	2.30
11	16.32	[1 3 3]	1.29
12	51.54	[1 2 2]	1.32
13	57.59	[2 5 5]	2.11
14	51.55	[2 4 5]	3.33
15	17.00	[0 1 7]	0.00
16	17.80	[0 3 8]	0.00

Table CVI. Parent-Twin Misorientation List for Experimental Orientation Relationship Applying Cubic Symmetry

Δg_i	$\theta(\Delta g_i)$ (deg)	\vec{r}	$\delta(\Delta g_i)$ (deg)	Δg_i	$\theta(\Delta g_i)$ (deg)	\vec{r}	$\delta(\Delta g_i)$ (deg)
17	57.28	[5 5 6]	0.85	45	18.68	[3 3 5]	0.66
18	53.62	[0 1 1]	0.25	46	22.31	[2 3 7]	1.85
19	3.19	[3 3 7]	0.87	47	40.86	[4 5 6]	2.17
20	6.93	[3 5 5]	0.80	48	41.83	[1 1 1]	0.44
21	51.90	[1 5 6]	2.47	49	53.72	[1 5 6]	2.57
22	50.74	[1 3 3]	2.39	50	53.47	[3 4 6]	2.29
23	57.03	[2 6 7]	0.83	51	50.56	[2 4 5]	1.71
24	58.13	[1 5 5]	0.82	52	47.49	[1 6 6]	1.71
25	19.93	[0 1 5]	3.01	53	49.65	[0 4 5]	0.58
26	20.11	[1 2 8]	2.94	54	26.00	[1 2 7]	1.36
27	49.57	[1 1 1]	2.99	55	26.91	[1 3 8]	1.42

Table CVI. continued

Δg_i	$\theta(\Delta g_i)$ (deg)	\vec{r}	$\delta(\Delta g_i)$ (deg)	Δg_i	$\theta(\Delta g_i)$ (deg)	\vec{r}	$\delta(\Delta g_i)$ (deg)
28	48.79	[4 5 6]	0.22	56	48.56	[3 4 6]	1.10
29	15.54	[0 3 7]	1.73	57	29.33	[3 3 7]	1.08
30	11.15	[2 4 5]	0.32	58	37.83	[2 3 3]	1.68
31	51.66	[2 5 6]	0.67	59	43.70	[3 5 5]	2.72
32	57.66	[2 4 5]	0.63	60	26.83	[1 1 5]	0.67
33	13.14	[1 4 5]	1.54	61	38.86	[4 5 5]	1.89
34	17.90	[1 2 3]	2.50	62	50.90	[1 5 7]	1.50
35	50.99	[3 5 5]	2.33	63	49.68	[3 4 8]	2.43
36	51.70	[3 3 4]	2.06	64	44.99	[0 6 7]	0.18
37	54.61	[2 5 5]	1.26	65	32.05	[2 2 9]	0.44
38	48.54	[2 5 5]	2.29	66	32.23	[0 2 7]	0.44
39	54.35	[2 3 4]	1.24	67	43.91	[3 4 7]	2.23
40	52.78	[2 2 3]	0.90	68	37.88	[4 4 7]	0.27
41	23.38	[3 4 7]	0.88	69	36.70	[1 1 9]	0.00
42	17.38	[2 2 3]	0.80	70	36.30	[1 1 9]	3.10
43	40.42	[2 5 5]	2.58	71	49.81	[1 1 2]	1.15
44	46.50	[1 3 3]	1.40				

Table CVII. Twin-Twin Misorientation List for Experimental Orientation Relationship Using Cubic Symmetry

Δg_i	$\theta(\Delta g_i)$ (deg)	\vec{r}	$\delta(\Delta g_i)$ (deg)	Δg_i	$\theta(\Delta g_i)$ (deg)	\vec{r}	$\delta(\Delta g_i)$ (deg)
72	27.85	[1 3 7]	1.03	150	31.29	[3 4 7]	1.39
73	29.15	[1 4 8]	0.97	151	31.47	[4 4 5]	0.00
74	51.26	[2 3 4]	1.42	152	52.44	[0 5 6]	0.89
75	47.47	[2 4 5]	1.50	153	53.97	[0 1 1]	2.56
76	46.40	[0 6 7]	2.86	154	28.76	[4 5 5]	0.82
77	48.93	[0 5 7]	2.77	155	30.95	[3 3 5]	2.44
78	43.57	[1 3 3]	1.60	156	36.40	[0 5 8]	2.74
79	37.51	[2 5 6]	2.51	157	30.75	[1 4 8]	1.21
80	19.19	[3 5 6]	1.68	158	26.18	[1 3 6]	0.84
81	25.33	[3 5 7]	1.83	159	31.83	[1 4 6]	0.53
82	54.79	[4 5 7]	2.03	160	55.66	[1 5 6]	0.71
83	56.60	[2 3 4]	1.38	161	54.33	[2 5 6]	0.36
84	24.58	[2 2 5]	0.64	162	33.20	[0 1 1]	1.82
85	21.43	[3 4 5]	2.23	163	35.86	[1 5 5]	0.82
86	54.57	[1 5 7]	3.46	164	42.00	[2 5 5]	1.93
87	52.32	[1 6 6]	1.30	165	38.51	[1 5 5]	1.64
88	38.94	[1 1 1]	2.18	166	44.43	[0 1 2]	2.58
89	38.07	[2 2 3]	1.92	167	47.93	[1 3 7]	1.72
90	51.18	[2 6 7]	1.37	168	31.80	[1 1 3]	0.50
91	57.28	[2 6 7]	2.09	169	49.11	[0 2 3]	2.07
92	46.63	[1 1 1]	1.57	170	49.94	[0 5 6]	1.21
93	48.62	[3 3 4]	1.23	171	31.95	[3 5 5]	1.67
94	15.89	[1 5 7]	3.10	172	37.96	[0 1 1]	1.54
95	14.07	[1 2 2]	1.24	173	42.28	[1 6 7]	1.51
96	31.95	[2 2 7]	1.70	174	40.90	[1 3 4]	1.03
97	32.02	[1 3 8]	2.86	175	36.08	[1 6 7]	1.73
98	52.02	[3 3 4]	1.52	176	41.13	[1 2 8]	2.09
99	47.61	[3 4 5]	1.00	177	45.83	[0 1 4]	3.34
100	42.19	[0 6 7]	1.90	178	36.78	[1 5 7]	1.77
101	44.68	[1 6 7]	1.85	179	41.48	[0 5 8]	1.34
102	43.07	[3 5 5]	1.86	180	43.80	[1 4 7]	0.96
103	37.37	[4 5 6]	1.33	181	38.66	[0 2 3]	2.20
104	24.19	[3 4 5]	2.56	182	40.20	[0 1 7]	0.58
105	29.99	[4 4 7]	1.05	183	44.60	[0 1 9]	2.23
106	50.59	[3 4 6]	2.88	184	34.28	[0 0 1]	0.00
107	52.39	[1 2 3]	0.90	185	34.90	[1 1 7]	0.46
108	26.20	[1 2 7]	1.11	186	33.91	[3 4 7]	2.48
109	22.16	[1 2 4]	2.62	187	33.16	[2 3 6]	1.50
110	51.14	[0 3 5]	3.09	188	52.87	[5 5 6]	1.81
111	48.22	[1 5 7]	1.94	189	47.82	[4 5 6]	2.46

Table CVII. continued

Δg_i	$\theta(\Delta g_i)$ (deg)	\vec{r}	$\delta(\Delta g_i)$ (deg)	Δg_i	$\theta(\Delta g_i)$ (deg)	\vec{r}	$\delta(\Delta g_i)$ (deg)
112	40.84	[3 3 4]	2.48	190	34.51	[1 6 7]	2.77
113	38.94	[3 4 4]	2.01	191	36.76	[0 6 7]	2.93
114	47.76	[1 3 3]	1.16	192	43.93	[3 3 5]	1.20
115	54.01	[2 6 7]	1.08	193	38.94	[4 5 7]	1.03
116	50.41	[3 4 4]	1.17	194	28.83	[4 4 5]	0.45
117	19.13	[1 2 2]	0.00	195	33.86	[4 5 5]	2.47
118	42.58	[3 5 7]	1.68	196	49.33	[0 5 8]	0.24
119	48.29	[3 4 6]	2.71	197	47.99	[1 4 6]	1.53
120	39.65	[1 3 3]	0.95	198	39.00	[3 4 6]	2.62
121	36.78	[3 5 6]	2.04	199	38.69	[1 2 3]	0.32
122	35.21	[0 2 7]	2.10	200	42.48	[3 3 4]	0.41
123	29.79	[0 2 5]	2.65	201	30.43	[0 6 7]	2.58
124	37.20	[3 4 7]	1.69	202	33.64	[1 3 4]	1.77
125	43.19	[1 1 2]	1.45	203	38.94	[3 4 7]	2.02
126	45.92	[2 6 7]	0.74	204	34.48	[1 2 3]	2.20
127	42.72	[1 2 2]	1.05	205	39.09	[4 5 5]	1.71
128	34.25	[1 1 6]	0.74	206	44.68	[1 5 7]	1.73
129	28.20	[1 2 9]	0.00	207	43.87	[1 2 3]	1.23
130	52.88	[1 4 6]	1.31	208	43.71	[1 6 6]	0.05
131	55.81	[2 6 7]	0.52	209	48.36	[2 6 7]	1.08
132	38.94	[0 0 1]	3.34	210	46.74	[1 1 4]	0.61
133	39.48	[1 1 9]	2.48	211	42.36	[0 2 5]	3.19
134	52.91	[1 2 3]	1.90	212	31.86	[0 1 2]	2.08
135	49.28	[2 3 6]	0.92	213	37.33	[1 3 7]	0.46
136	22.82	[0 2 9]	0.32	214	45.16	[0 1 5]	0.39
137	22.48	[0 1 5]	0.53	215	38.94	[0 1 7]	1.24
138	37.30	[1 6 7]	1.56	216	42.56	[2 5 5]	0.57
139	31.14	[1 4 5]	0.49	217	47.56	[3 5 6]	1.70
140	23.20	[1 6 7]	0.00	218	37.05	[0 1 2]	0.70
141	29.46	[1 6 6]	1.27	219	35.44	[1 2 5]	0.00
142	59.98	[1 5 5]	0.70	220	41.39	[2 3 8]	1.54
143	58.86	[1 3 3]	1.29	221	32.86	[0 1 9]	2.03
144	32.21	[0 5 8]	2.12	222	36.83	[1 1 3]	0.22
145	34.72	[2 5 7]	1.35	223	32.48	[1 2 5]	1.11
146	43.95	[2 4 5]	0.99	224	38.46	[1 2 2]	0.47
147	40.59	[1 3 4]	1.09	225	39.20	[1 4 4]	0.55
148	47.46	[1 5 7]	3.61	226	27.63	[2 2 7]	0.95
149	50.84	[1 4 7]	1.92	227	40.96	[0 1 1]	0.25

**APPENDIX D: KS-TETRAGONAL ORIENTATION
RELATIONSHIP MISORIENTATION DATA**

See Tables DVIII, DIX, DX.

Table DVIII. Intra-parent Misorientation List for KS Orientation Relationship with Respect to Tetragonal Symmetry

Δg_i	$\theta(\Delta g_i)$ (deg)	\vec{r}	$\delta(\Delta g_i)$ (deg)
0	0.00	[1 0 0]	0.00
1	10.53	[1 0 1]	0.08
2	76.27	[5 5 1]	0.82
3	70.53	[1 1 0]	0.08
4	82.82	[3 3 1]	0.39
5	71.21	[7 5 0]	0.57
6	77.65	[7 5 1]	0.98
7	14.88	[8 3 1]	2.93
8	10.53	[1 1 1]	0.76
9	90.00	[6 5 1]	2.69

Table DVIII. continued

Δg_i	$\theta(\Delta g_i)$ (deg)	\vec{r}	$\delta(\Delta g_i)$ (deg)
10	84.26	[7 6 1]	3.18
11	20.60	[5 5 3]	1.79
12	83.14	[5 4 0]	0.92
13	90.00	[7 6 1]	2.28
14	85.62	[3 2 0]	2.28
15	20.60	[3 0 1]	1.27
16	21.06	[7 3 0]	0.96

Table DIX. Parent-Twin Misorientation List for KS Orientation Relationship with Tetragonal Symmetry

Δg_i	$\theta(\Delta g_i)$ (deg)	\vec{r}	$\delta(\Delta g_i)$ (deg)	Δg_i	$\theta(\Delta g_i)$ (deg)	\vec{r}	$\delta(\Delta g_i)$ (deg)
17	60.00	[1 0 1]	0.08	45	66.84	[5 2 3]	2.59
18	60.00	[1 1 1]	0.00	46	79.33	[4 0 1]	0.57
19	49.47	[1 0 1]	0.08	47	70.53	[6 0 1]	3.04
20	90.00	[1 0 0]	0.00	48	77.17	[6 1 3]	1.37
21	90.48	[8 0 1]	0.46	49	73.21	[6 0 3]	0.45
22	50.51	[4 1 5]	1.89	50	55.23	[4 1 4]	1.34
23	47.11	[5 2 4]	2.28	51	56.04	[7 1 5]	0.80
24	57.21	[6 2 5]	0.73	52	57.28	[7 2 4]	1.33
25	57.21	[5 3 6]	0.28	53	45.80	[6 1 7]	1.20
26	70.53	[9 1 1]	3.65	54	51.32	[5 0 8]	0.74
27	71.21	[9 1 1]	1.50	55	65.68	[8 1 0]	2.55
28	70.53	[1 1 1]	0.00	56	65.82	[9 1 2]	1.22
29	71.21	[4 3 3]	1.28	57	60.00	[5 0 3]	2.46
30	76.27	[9 1 0]	3.74	58	65.68	[3 1 0]	0.40
31	84.26	[9 0 1]	0.53	59	72.16	[7 0 3]	2.54
32	58.90	[7 2 4]	1.44	60	68.84	[7 1 4]	0.72
33	57.21	[6 3 5]	0.28	61	62.19	[9 0 1]	1.52
34	85.62	[8 1 1]	0.77	62	80.13	[6 0 3]	1.50
35	77.65	[9 2 1]	2.84	63	49.19	[7 1 5]	1.22
36	65.82	[4 1 3]	1.80	64	51.73	[6 0 3]	2.15
37	60.83	[3 0 2]	1.32	65	40.28	[5 0 4]	0.92
38	67.12	[5 2 4]	0.83	66	58.37	[9 2 0]	3.13
39	68.83	[8 2 5]	0.00	67	57.28	[7 1 1]	1.26
40	60.00	[5 1 4]	0.38	68	60.00	[8 1 4]	1.69
41	64.21	[6 0 5]	0.68	69	64.21	[3 0 1]	1.00
42	73.10	[9 2 1]	2.25	70	51.80	[5 0 1]	0.16
43	80.13	[6 1 0]	0.63	71	51.32	[9 1 0]	2.30
44	70.22	[5 1 2]	0.87	72	57.28	[3 0 2]	0.91

Table DX. Twin-Twin Misorientation List Applying KS Orientation Relationship with Tetragonal Symmetry

Δg_i	$\theta(\Delta g_i)$ (deg)	\vec{r}	$\delta(\Delta g_i)$ (deg)	Δg_i	$\theta(\Delta g_i)$ (deg)	\vec{r}	$\delta(\Delta g_i)$ (deg)
73	89.37	[7 1 2]	0.83	151	30.26	[4 3 7]	0.69
74	88.41	[8 3 1]	1.01	152	28.41	[1 1 1]	0.00
75	55.61	[6 3 5]	1.05	153	67.12	[5 3 3]	0.97
76	49.19	[7 2 5]	1.27	154	58.16	[6 4 3]	1.85
77	67.12	[8 3 4]	0.44	155	75.34	[5 2 0]	0.75
78	73.10	[7 4 4]	1.21	156	78.62	[7 3 1]	1.15
79	47.56	[6 2 7]	2.78	157	39.87	[4 0 7]	2.11
80	37.24	[6 2 7]	1.60	158	29.87	[3 0 7]	0.92
81	82.82	[6 0 1]	1.38	159	88.45	[7 1 2]	0.93
82	84.80	[3 0 1]	2.03	160	90.00	[7 1 3]	0.62
83	54.84	[5 4 4]	1.33	161	67.84	[7 5 4]	1.03
84	55.61	[6 5 3]	1.05	162	69.41	[5 4 2]	2.38
85	81.62	[8 2 1]	0.98	163	92.92	[5 0 2]	0.28
86	79.33	[4 1 0]	0.57	164	89.07	[6 3 0]	1.77
87	53.51	[5 2 3]	2.22	165	45.10	[6 2 7]	1.20
88	63.26	[7 3 5]	0.90	166	38.63	[1 0 1]	0.79

Table DX. continued

Δg_i	$\theta(\Delta g_i)$ (deg)	\vec{r}	$\delta(\Delta g_i)$ (deg)	Δg_i	$\theta(\Delta g_i)$ (deg)	\vec{r}	$\delta(\Delta g_i)$ (deg)
89	38.94	[1 1 1]	0.00	167	81.13	[7 3 3]	0.60
90	40.28	[4 3 6]	2.35	168	86.95	[7 4 3]	1.11
91	68.84	[5 3 2]	1.64	169	34.36	[2 2 9]	0.52
92	65.82	[6 5 3]	1.84	170	76.43	[6 3 4]	2.29
93	49.47	[1 1 1]	0.00	171	67.12	[2 1 1]	0.49
94	50.51	[3 2 2]	1.39	172	80.91	[5 2 0]	0.45
95	90.00	[9 1 2]	3.42	173	67.69	[8 2 3]	2.23
96	84.26	[9 1 0]	0.53	174	67.84	[7 3 2]	0.77
97	84.80	[8 2 3]	1.05	175	63.93	[6 1 3]	0.95
98	94.25	[5 1 2]	0.52	176	68.01	[8 2 3]	2.76
99	54.84	[5 4 4]	1.33	177	54.92	[8 2 1]	2.61
100	47.56	[6 3 4]	2.10	178	46.95	[8 3 1]	3.26
101	62.19	[3 1 1]	1.20	179	77.00	[7 2 3]	1.29
102	67.12	[8 4 3]	0.44	180	76.62	[7 3 3]	1.28
103	44.35	[5 3 5]	1.45	181	54.21	[7 1 3]	1.48
104	34.85	[5 4 5]	1.15	182	59.08	[9 2 2]	0.24
105	77.17	[8 1 2]	1.49	183	52.83	[9 0 1]	2.76
106	80.41	[7 1 3]	0.80	184	45.10	[8 1 0]	1.44
107	47.56	[6 4 3]	2.10	185	58.60	[1 0 0]	2.92
108	49.19	[7 5 2]	1.27	186	59.08	[6 1 0]	0.96
109	90.00	[4 1 1]	2.56	187	75.87	[5 1 2]	1.31
110	86.85	[8 2 1]	2.77	188	85.47	[7 1 3]	0.80
111	47.83	[8 3 3]	2.17	189	57.94	[5 5 6]	0.39
112	57.28	[6 2 3]	0.87	190	49.43	[4 3 4]	1.73
113	40.28	[6 4 3]	2.35	191	68.27	[7 1 2]	1.49
114	38.94	[3 2 3]	0.76	192	72.16	[3 1 1]	0.22
115	63.26	[5 3 1]	0.45	193	47.91	[4 4 7]	2.13
116	58.90	[6 5 2]	1.41	194	38.94	[5 4 7]	1.00
117	51.73	[5 5 3]	1.79	195	69.41	[7 0 2]	1.13
118	84.26	[4 0 1]	0.70	196	71.99	[7 0 3]	1.68
119	76.27	[7 4 2]	2.50	197	52.60	[8 3 4]	0.00
120	78.90	[5 4 1]	1.64	198	52.79	[7 3 2]	1.19
121	67.12	[5 2 1]	0.52	199	77.89	[7 1 4]	0.96
122	73.10	[7 3 0]	3.05	200	81.76	[5 4 3]	1.63
123	35.45	[3 1 0]	1.81	201	40.28	[5 5 6]	0.00
124	29.12	[6 3 1]	2.27	202	73.69	[5 1 1]	2.00
125	81.62	[7 3 1]	0.62	203	77.14	[5 2 1]	0.93
126	83.97	[7 4 1]	0.72	204	38.94	[4 3 7]	0.41
127	62.19	[6 3 2]	1.89	205	30.93	[5 2 6]	0.79
128	67.12	[7 4 1]	0.33	206	75.34	[8 0 5]	0.24
129	34.85	[6 1 2]	1.33	207	56.60	[7 3 2]	0.08
130	26.11	[7 2 1]	0.77	208	58.37	[8 4 1]	2.88
131	79.33	[5 4 2]	0.83	209	66.00	[5 2 2]	2.05
132	71.88	[5 5 2]	0.93	210	67.12	[3 2 1]	0.99
133	38.94	[9 1 1]	3.65	211	50.27	[3 1 0]	0.61
134	40.28	[5 1 1]	1.35	212	43.87	[6 3 1]	1.22
135	75.36	[4 3 1]	2.00	213	82.11	[4 1 1]	1.21
136	83.08	[3 2 1]	1.85	214	82.45	[8 3 2]	1.18
137	20.60	[3 1 0]	1.27	215	47.91	[7 0 2]	0.68
138	21.06	[7 0 3]	0.96	216	38.94	[6 0 1]	3.04
139	38.33	[1 0 1]	3.21	217	67.12	[6 3 1]	2.07
140	27.82	[6 1 6]	2.59	218	69.63	[6 4 1]	0.74
141	90.00	[7 0 2]	0.53	219	36.92	[3 2 0]	0.91
142	92.48	[7 0 3]	0.92	220	86.14	[8 3 2]	1.59
143	59.55	[5 5 3]	1.84	221	87.31	[7 4 2]	0.94
144	61.99	[3 3 1]	1.40	222	30.93	[1 0 0]	1.15
145	93.46	[7 3 1]	0.90	223	40.28	[1 1 4]	1.39
146	85.91	[8 4 1]	1.05	224	31.96	[3 1 8]	1.27
147	45.54	[7 3 5]	0.73	225	79.91	[2 0 1]	1.04
148	39.87	[7 1 4]	1.25	226	83.79	[5 5 3]	1.53
149	72.16	[7 4 3]	2.14	227	22.75	[2 2 9]	0.83
150	78.40	[7 5 3]	1.77	228	86.44	[5 5 2]	0.65

APPENDIX E: SIMILAR MISORIENTATION COMPARISONS

See Table EXI.

Table EXI. The Possible Misorientation Pairs That may be Indistinguishable Upon Experimental Observation

OR	Δg_i	Δg_j	$\Delta\theta(\Delta g_{i,j})$ (deg)	$\Delta \vec{r}(\Delta g_{i,j})$ (deg)
KS-Cubic	39	136	0.619	0.409
KS-Cubic	50	77	0.309	0.909
KS-Cubic	84	87	0.670	0.115
Low-C Expt.	59	102	0.630	0.772
Low-C Expt.	61	205	0.229	0.010
Low-C Expt.	147	174	0.315	0.725
KS-Tetrag.	62	225	0.223	0.492
KS-Tetrag.	139	166	0.309	0.909
KS-Tetrag.	142	163	0.441	0.354
KS-Tetrag.	173	176	0.315	0.532

KS-cubic refers to KS orientation relationship assuming cubic symmetry, low-C expt. is the referenced experimental orientation relationship, and KS-tetrag is the KS orientation relationship assuming tetragonal symmetry.

ELECTRONIC SUPPLEMENTARY MATERIAL

The online version of this article (<https://doi.org/10.1007/s11661-018-4977-5>) contains supplementary material, which is available to authorized users.

REFERENCES

1. S. Morito, H. Tanaka, R. Konishi, and T. Maki: *Acta Mater.*, 2003, vol. 51, pp. 1789–99.
2. H. Kitahara, R. Ueji, N. Tsuji, and Y. Minamino: *Acta Mater.*, 2006, vol. 54, pp. 1279–88.
3. G. Krauss: *Hardenability Concepts with Applications to Steel*, AIME, Warrendale, PA, 1978, pp. 229–48.
4. G. Krauss and A.R. Marder: *Metall. Trans.*, 1971, vol. 2, pp. 2343–57.
5. A.R. Marder and G. Krauss: *ASM Trans.*, 1967, vol. 60, pp. 651–60.
6. V.A. Yardley, E.J. Payton, T. Matsuzaki, R. Sugiura, A.T. Yokobori Jr., S. Tsurekawa, Y. Hasegawa, Creep and Fracture of Engineering Materials and Structures. Proc. 12th Int. Conf. Creep and Fracture of Eng. Mater. and Struct. (JIMIS 11), held at Kyoto TERRSA, Kyoto, Japan, May 27–31, 2012, Edited by: K. Maruyama, F. Abe, M. Igarashi, K. Kishida, M. Suzuki, K. Yoshimi, The Jap. Ins. of Met, Sendai, 2012, paper C14.
7. K. Kimura, N. Ohi, K. Shimazu, and T. Matsuo: *Scr. Mater.*, 1987, vol. 21, pp. 19–22.
8. V.A. Yardley, S. Fahimi, and E.J. Payton: *Mater. Sci. Technol.*, 2015, vol. 31, pp. 547–53.
9. S.H. Hong and J. Yu: *Scr. Mater.*, 1989, vol. 23, pp. 1057–62.
10. S. Matsuda, T. Inoue, H. Mimura, Y. Okamura, Climax Molybdenum Development Company, Ltd., Japan, 1971, pp. 45–66.
11. Z. Guo, C.S. Lee, and J.W. Morris: *Acta. Mater.*, 2004, vol. 52 (19), pp. 5511–18.
12. S. Morito, H. Yoshida, T. Maki, and X. Huang: *J. Mater. Sci. Eng. A*, 2006, vols. 438–440, pp. 237–40.
13. S.K. Banerji, C.J. McMahon, Jr., and H.C. Feng: *Metall. Trans. A*, 1978, vol. 9A, pp. 237–47.
14. R.M. Horn and R.O. Ritchie: *Metall. Trans. A*, 1978, vol. 9A, pp. 1039–53.
15. Z. Nishiyama: *Sci. Rep., Tohoku Imperial Univ.*, vol. 23, pp. 637–64 (1934).
16. G. Wassermann: Über den Mechanismus der $\alpha \rightarrow \gamma$ Umwandlung des Eisens (On the Mechanism of the $\alpha \rightarrow \gamma$ Transformation of Iron). Mitteilungen aus dem Kais. Wilhelm. Inst. für Eisenforsch., vol. 17, pp. 149–55 (1935).
17. G. Kurdjumow, G. Sachs: *Z. Physik*, vol. 64, pp. 325–43 (1930).
18. J.W. Cahn, G. Kalonji: *Proc. Int. Conf. Solid-Solid Phase Trans.* Edited by: H.I. Aaronson, D.E. Laughlin, R.F. Sekerka and C.M. Wayman., The Met. Soc. of AIME (1982).
19. A.B. Greninger and A.R. Troiano: *Metall. Trans.*, 1949, vol. 185, pp. 590–98.
20. M.S. Wechsler, D.S. Lieberman, and T.A. Read: *Trans. AIME*, 1953, vol. 197, pp. 1503–15.
21. J.S. Bowles and JK Mackenzie: *Acta. Metall.*, 1954, vol. 2, pp. 129–37.
22. J.K. Mackenzie and J.S. Bowles: *Acta. Metall.*, 1954, vol. 2, pp. 138–47.
23. J.S. Bowles and J.K. Mackenzie: *Acta. Metall.*, 1954, vol. 2, pp. 224–34.
24. J.K. Mackenzie and J.S. Bowles: *Acta. Metall.*, 1957, vol. 5, pp. 137–49.
25. J.S. Bowles and J.K. Mackenzie: *Acta Metall.*, 1962, vol. 10, pp. 625–36.
26. Z. Nishiyama, M.E. Fine, C.M. Wayman: *Martensitic Transformation*, Materials Science and Technology. Academic Press, New York, 1978.
27. C.M. Wayman: *Introduction to the Crystallography of Martensitic Transformations*. Macmillan, Macmillan Series in Materials Science, Macmillan, New York, 1964.
28. H. Kitahara, R. Ueji, M. Ueda, N. Tsuji, and Y. Minamino: *Mater. Charact.*, 2005, vol. 54, pp. 378–86.
29. M. Nikravesh, M. Naderi, and G.H. Akbari: *Mater. Sci. Eng.*, 2012, vol. 540, pp. 24–29.
30. O. Sherby, J. Wadsworth, D. Lesuer, C. Syn: The c/a Ratio in Quenched Fe-C and Fe-N steels—A Heuristic Story. THERMEC, Vancouver, Canada, July 4–July 8 (2006).
31. V. Sinha, E.J. Payton, M. Gonzales, R.A. Abrahams, and BS Song: *Metallogr., Microstruct. Anal.*, 2017, vol. 6 (6), pp. 610–18.
32. E.J. Payton, A. Aghajani, F. Otto, G. Eggler, and V.A. Yardley: *Scr. Mater.*, 2012, vol. 66, pp. 1045–48.
33. C. Cayron: *Acta Crystallogr.*, 2006, vol. 62 (Pt 1), pp. 21–40.
34. V.A. Yardley and E.J. Payton: *Mater. Sci. Technol.*, 2014, vol. 30, pp. 1125–30.
35. M. Natori, Y. Futamura, T. Tsuchiyama, and S. Takaki: *Scr. Mater.*, 2005, vol. 53, pp. 603–08.
36. M. Abbasi, T.W. Nelson, and C.D. Sorensen: *J. Appl. Crystallogr.*, 2013, vol. 46, pp. 716–25.
37. M. Abbasi, D.I. Kim, T.W. Nelson, and M. Abbasi: *Mater. Charact.*, 2014, vol. 95, pp. 219–31.
38. G. Miyamoto, N. Iwata, N. Takayama, and T. Furuhara: *Acta Mater.*, 2010, vol. 58, pp. 6393–6403.
39. S. Cluff, T. Nelson, R. Song, D. Fullwood, IOP Conf. Ser. Mater. Sci. Eng., vol. 375 (2018).
40. A. Heinz and P. Neumann: *Acta. Crstallogr. A*, 1991, vol. A47, pp. 780–89.
41. J.W. Christian: *Jour. Phys. Colloq.*, 1974, vol. 35 (C7), pp. 65–76.
42. V. Randle, G.S. Rohrer, H.M. Miller, M. Coleman, and G.T. Owen: *Acta Mater.*, 2008, vol. 10, pp. 2363–73.
43. M.A. Bingham, B.K. Lograsso, and F.C. Laabs: *ULTRD6*, 2010, vol. 110, pp. 1312–19.
44. Y.H. Chen, S.U. Park, D. Wei, G. Newstadt, M. Jackson, J.P. Simmons, M. De Graef, and A.O. Hero: *Microsc. Microanal.*, 2015, vol. 21, pp. 1–14.